




Published by Avanti Publishers  
**Journal of Advanced Thermal  
Science Research**

ISSN (online): 2409-5826



# Selective Laser Sintering: Processing, Materials, Challenges, Applications, and Emerging Trends

Bin Xiao <sup>1,\*</sup> and Zhangxiang Ye<sup>2</sup>

<sup>1</sup>Department of Engineering Technology, Texas State University, San Marcos, TX 78666, USA

<sup>2</sup>School of Civil Engineering and Architecture, Zhejiang Sci-Tech University, Hangzhou, Jiangsu 310018, P.R. China

## ARTICLE INFO

*Article Type:* Research Article

*Academic Editor:* Dunxi Yu

*Keywords:*

SLS

Materials

Processing

Challenges

Applications and Emerging Trends

*Timeline:*

Received: October 30, 2024

Accepted: December 06, 2024

Published: December 18, 2024

*Citation:* Xiao B, Ye Z. Selective laser sintering: Processing, materials, challenges, applications, and emerging trends. J Adv Therm Sci Res. 2024; 11: 65-99.

*DOI:* <https://doi.org/10.15377/2409-5826.2024.11.4>

## ABSTRACT

Selective laser sintering (SLS) has revolutionized manufacturing by enabling the production of intricate designs with enhanced flexibility and material efficiency. The present review delves into the SLS process, its compatibility with materials such as polymers, metals, and composites, and its influence on microstructure, mechanical properties, and overall performance. It addresses challenges like dimensional accuracy, surface finish, and residual stress while highlighting applications across various industries. Additionally, the review explores emerging trends, including hybrid manufacturing and the integration of artificial intelligence, to shape future developments in SLS technology.

\*Corresponding Author

Email: [b\\_x3@txstate.edu](mailto:b_x3@txstate.edu)

Tel: +(1) 281-881-1665

# 1. Introduction

Selective Laser Sintering (SLS), pioneered by Dr. Carl Deckard [1], uses a computer-controlled laser to selectively sinter powdered materials, constructing parts layer by layer. As illustrated in Fig. (1), the laser fuses material only within the designated part boundaries, scanning each layer until the structure is fully formed. Powders are evenly distributed across the building area using a drum, while a temperature control system ensures consistent sintering conditions throughout the process [2]. SLS has transformed manufacturing by enabling the direct production of complex parts from digital models, offering exceptional design flexibility and material efficiency [3-10]. Zhang *et al.* [3] used SLS to fabricate CF/PEEK composites with various process parameters, achieving high failure strength. Wu *et al.* [4] demonstrated that superhydrophobic, abrasion-resistant objects can be SLS printed using hydrophobic-fumed-silica (HFS)/polymer composite grains, maintaining anti-wetting properties even after multiple abrasion tests. Zhang *et al.* [5] incorporated carbonyl iron as a magnetic and heat-conductive additive to 3D print oral tablets containing isoniazid, an antitubercular drug. They optimized tablet quality by adjusting printing parameters and showed that magnetic nanoparticles improve the sintering process. Deng *et al.* [6] fabricated resin-ceramic-based  $\text{Fe}_3\text{O}_4$ /graphite composites using SLS and vacuum impregnation, demonstrating that adjusting laser power balances absorption and mechanical properties. Wu *et al.* [7] printed alumina-based ceramics with superhydrophilic properties and strong resistance to moisture-thermal transitions. Their "I-shaped" evaporators exhibited salt resistance and maintained high evaporation efficiency in seawater and 20 wt% brine. Xue *et al.* [8] developed a parametric method to design TPMS lattice structures with adjustable elastic modulus using simulations. They fabricated a flexible TPMS lattice with SLS thermoplastic polyurethane and found that its geometric shape and volume fraction significantly impact mechanical properties. Choudhury *et al.* [9] studied how laser power and hatch spacing affect particle fusion in SLS. They examined the physicochemical and mechanical properties of sintered objects made with dapsone and poly, showing that laser parameters influence the final object's properties. Ghaltaghchyan *et al.* [10] used SLS to manufacture silicon carbide-based composite ceramics and studied how sintering parameters and raw materials affect sinterability, optimizing the process for improved results.

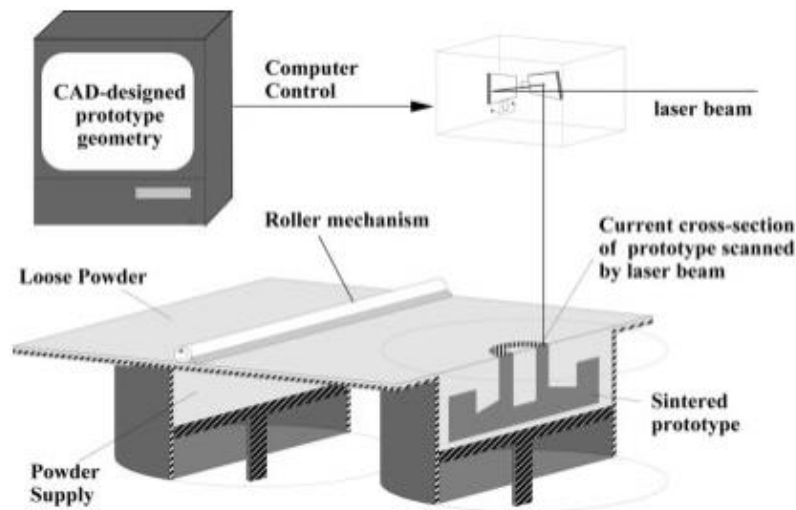


**Figure 1:** Schematic representation of a typical SLS setup [2].

SLS uses a laser to fuse powdered materials into solid layers without fully melting them, reducing thermal stress and enabling complex geometries. Material selection is key, affecting strength, stability, and surface quality [11-15]. Han *et al.* [11] reviewed SLS polymer processing, covering key parameters, materials, applications, and future research. Hassan *et al.* [12] printed thermoset resin parts with high dimensional stability and a glass transition temperature of  $\sim 300^\circ\text{C}$ . Fully crosslinked thermosets had 900% higher compressive strength than uncured parts. Shi *et al.* [13] found that lower melt viscosity improves density, while higher crystallinity increases shrinkage, reducing precision. Smaller particle sizes enhance both precision and density. Gibson and Shit [14] discussed how powder properties impact fabrication and mechanical performance, noting that post-processing also affects final part quality. Tiwari *et al.* [15] analyzed material selection for SLS in engineering, medicine, and

other fields, emphasizing the importance of optimizing process parameters and material choices for better quality and sustainability.

Originally developed for polymers, SLS now includes metals and composites, making it useful in aerospace, automotive, and healthcare industries [16-25]. Storch *et al.* [16] compared sintered metals like EOS DirectSteel 20 and 3D Laser Form ST100 to traditional automotive materials. Elbadawi *et al.* [17] introduced Cold Laser Sintering (CLS), which fuses particles using only laser energy, reducing carbon emissions by 99% while maintaining similar properties to SLS. Williams and Revington [18] used an SLS machine to create a precise model of an orbital blowout fracture for medical applications. Lv *et al.* [19] studied fire-retardant polyetherimide powders for SLS, identifying optimal laser settings for strong mechanical properties. Quincieu *et al.* [20] demonstrated the benefits of using SLS to create a full-scale modular satellite model for quality control, fit checks, and tooling design. Goulas and Friel [21] reviewed ceramic advancements for SLS in aerospace. Agarwala *et al.* [22] developed a strain sensor using laser-sintered silver nanoparticle ink, which remained stable over 700 bending cycles. Awad *et al.* [23] explored SLS 3D printing applications and challenges, particularly in pharmaceuticals. Fina *et al.* [24] tested SLS for 3D-printed medicines, confirming its effectiveness for drug release control. Tel [25] evaluated SLS for cranio-maxillofacial surgery, finding that SLS-printed materials are stronger and more sterilizable than stereolithography (SLA) prints, making them ideal for surgical guides.

Metals like aluminum and titanium offer high strength and durability for demanding applications [26-28], while composites provide lightweight strength and improved thermal properties [29-34]. Yan *et al.* [26] developed nylon-12-coated aluminum powders for selective laser sintering (SLS) to fabricate functional parts. Experimental results indicated that increasing the aluminum mass fraction from 0% to 50% improved dimensional accuracy, with tensile strength, flexural strength, and flexural modulus rising by 10.4%, 62.1%, and 122.3%, respectively, while elongation at break and impact strength declined by 65.0% and 74.4%. Furthermore, smaller aluminum particle sizes enhanced tensile strength, elongation at break, and impact strength. Subramanian *et al.* [27] found that binder-coated  $\text{Al}_2\text{O}_3$  particles in SLS produced stronger test bars than alumina-binder mixtures, with optimal strength at 20-40% binder content and laser energy density between 2-8 cal/cm<sup>2</sup>. Harada *et al.* [28] compared SLS-printed titanium parts to traditional cast specimens, finding that SLS parts matched or outperformed cast ones, with horizontally printed parts showing the highest tensile strength and smoothest surfaces. Yan *et al.* [29] printed a lightweight thermoplastic composite for flight vehicles, which was 40% lighter than metal alternatives and absorbed vibrations better. Özbay *et al.* [30] enhanced polyamide 12 (PA 12) with hollow glass microspheres (HGMs), reducing density while maintaining strength. Chen *et al.* [31] created strong SiC composites using SLS with carbon fiber and liquid silicon infiltration. Zhu *et al.* [32] developed carbon fiber/polyamide 12/epoxy (CF/PA12/EP) composites with high tensile and flexural strength. Azam *et al.* [33] reviewed SLS for polymer-based materials, focusing on process improvements and conductive polymer composites for strain-sensing applications. Yuan *et al.* [34] enhanced PA12 composites with  $\text{Al}_2\text{O}_3$  and BN particles, boosting thermal conductivity by 275% while maintaining good mechanical stability.

Despite its advantages, SLS faces challenges with part accuracy and quality control. Rapid heating and cooling can lead to surface roughness and residual stress [35-41]. Singh *et al.* [35] reviewed SLS challenges, covering process parameters, microstructure changes, defects, and surface roughness. Han *et al.* [36] discussed SLS for polymers, including principles, developments, and future directions. Petzold [37] studied the effects of laser power, roller speed, powder type, and scan spacing on surface roughness, using Focus Variation (FV) technology and ANOVA to analyze the results. Singh *et al.* [35] reviewed SLS challenges, covering process parameters, microstructure changes, defects, and surface roughness. Han *et al.* [36] discussed SLS for polymers, including principles, developments, and future directions. Petzold [37] studied the effects of laser power, roller speed, powder type, and scan spacing on surface roughness, using Focus Variation (FV) technology and ANOVA to analyze the results. Tonello *et al.* [38] examined surface roughness and grain size in curved SLS objects, finding that build setup, thin walls, and positioning impact quality. Sachdeva *et al.* [39] developed models to predict how laser power, scan spacing, and bed temperature influence surface roughness. Impey *et al.* [40] compared three methods for analyzing residual stress: neutron diffraction (non-destructive), the contour method (destructive), and Finite Element Analysis (theoretical). Van *et al.* [41] used SLS to create Ti6Al4V (ELI) samples, measuring residual stress with XRD and analyzing microstructure and principal stress values.

Recent research focuses on improving laser settings, scanning strategies, and post-processing methods like heat treatment and surface finishing to enhance part quality [42-43]. Lamikiz *et al.* [42] developed a laser polishing technique that melts and smooths the surface of sintered stainless steel and bronze parts, reducing roughness by 80.1% (from 7.5–7.8 $\mu\text{m}$  Ra to below 1.49 $\mu\text{m}$  Ra). The process created more uniform, harder surfaces without cracks or heat damage. Sanz and García [43] studied thermal and finishing treatments (shot peening and surface polishing) on DMLS parts made from Maraging Steel, Inconel 718, and CoCr alloy. They found that DMLS causes unwanted tensile stresses in Inconel 718 and CoCr but beneficial compressive stresses in Maraging Steel. Surface polishing further improved stress distribution and increased compressive residual stress. Real-time monitoring is also crucial for part integrity in SLS [44-46]. Chivel and Smurov [44] developed an optical system for tracking temperature during SLS/SLM processes, helping optimize sintering conditions. Gardner *et al.* [45] integrated optical coherence tomography (OCT) into SLS to detect surface and subsurface defects, using imaging techniques to identify heat irregularities. Zhang *et al.* [46] proposed an automatic laser control system that adjusts laser power based on presintering temperature using infrared cameras. Their system reduced temperature variations after sintering by up to 60% and 20% at different control levels, improving process consistency.

Current trends in SLS focus on integrating AI for optimizing parameters, predicting defects in real-time, and improving quality control [47, 48]. Hybrid manufacturing, which combines additive and subtractive processes, is also gaining popularity, allowing for high-precision parts with smoother surfaces [49, 50]. These advancements help overcome existing limitations, making SLS more suitable for critical applications across industries. Abdalla *et al.* [47] developed a deep learning model that predicts the printability of drug-loaded formulations with 90% accuracy. Their model also identifies key material properties that improve SLS printability, providing valuable insights for material optimization. Yehia *et al.* [48] analyzed the impact of processing variables on material properties and explored how machine learning (ML) techniques—supervised, unsupervised, and reinforcement learning—can optimize processes, detect defects, and enhance quality control. They highlighted challenges such as data availability and model interpretability but emphasized the benefits of combining ML with real-time monitoring and automated adjustments. In hybrid manufacturing, Lupone *et al.* [49] studied the electrical behavior of PA12-based composites before SLS processing. They found that adding graphite reduced flowability and mechanical strength but significantly improved electrical conductivity. However, no synergy was observed between graphite and carbon fiber reinforcement. Ferreira *et al.* [50] investigated how scan speed affects porosity and mechanical properties in hybrid SLS parts. They found that very high scan speeds (400–600 mm/s) increased porosity, reducing tensile strength and stiffness. While sintered and hybrid parts had similar tensile properties, hybrid parts showed lower fatigue strength over time compared to fully sintered specimens.

This review is organized as follows: Section 2 provides an overview of the mechanics of SLS. Section 3 explores the most common SLS processes for consolidating various powdered materials. Section 4 discusses studies on process parameters and their optimization. Section 5 reviews the key challenges and limitations of SLS. Section 6 highlights the applications of SLS in different industries. Section 7 examines emerging trends in recent research, and finally, Section 8 presents the conclusions based on the topics covered in this review.

## 2. SLS Overview and Process

SLS is an advanced additive manufacturing (AM) process that uses a high-energy laser to selectively fuse powdered material, building precise and complex 3D structures layer by layer [51, 52]. Leu *et al.* [51] explored laser sintering for making zirconium diboride (ZrB<sub>2</sub>) parts, optimizing parameters like laser power and scan speed. Goodridge *et al.* [52] reviewed polymer selection and processing for laser sintering, discussing challenges in material consistency and efforts to improve sintering materials.

The SLS process starts with a CAD model saved in STL format. The part's build orientation is chosen based on its function and strength needs. The model is sliced into layers, determining accuracy, build time, and the laser's scanning path. This data is then sent to the SLS machine for processing.

Once the design data is transferred to the machine's computer controller, the SLS process begins. Fig. (2) [53] illustrates a typical SLS workflow, which involves several complex physical phenomena that are crucial to producing high-quality components.

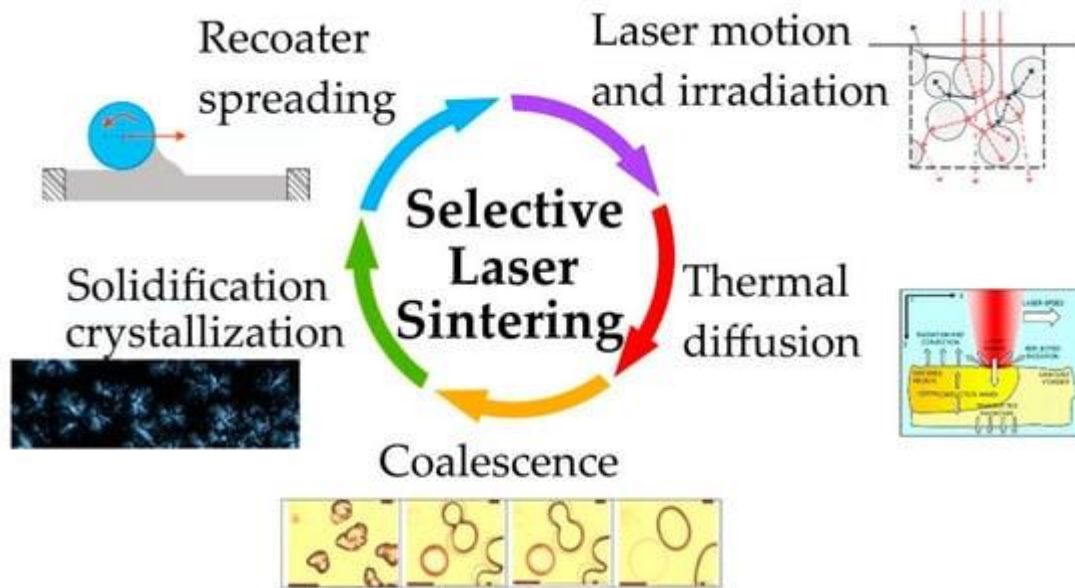


**Figure 2:** Illustration of SLS process [64].

### 2.1. Powder Spreading

A thin layer of powdered material is evenly distributed across the build platform using a roller or blade, forming the initial layer for laser sintering and subsequent layers. The powder bed is preheated to a specific temperature ( $T_b$ ) and maintained throughout the process. This ensures optimal sintering conditions. Achieving a continuous, defect-free, and homogenous powder layer is essential for fabricating dense, high-performance components. Several factors influence layer quality:

- Powder Properties: Particle size, distribution, and morphology directly affect the flowability of the powder.
- Recoater Design: The shape and interaction of the recoater, such as rollers, promote progressive particle rearrangement.
- Powder Dynamics: The interaction between the powder and the spreader, governed by various forces and mechanisms, requires precise control to ensure uniform deposition.

Miao *et al.* [54] conducted a literature review on powder spreading, examining how various factors influence powder bed quality. The study categorizes these factors into three groups: spreaders, spreading parameters, and feedstock powder properties. In addition to analyzing the individual effects of each factor, the review explores their interactions where relevant. Powder bed quality is evaluated based on density and surface condition.

### 2.2. Laser Motion and Irradiation

A high-powered laser, typically  $\text{CO}_2$  or fiber, scans the powder bed following a path determined by CAD data. The laser selectively sinters specific areas corresponding to the part's cross-section. The laser's energy raises the temperature of the powder above its sintering point while remaining below its melting point to ensure controlled sintering.

Yang *et al.* [55] presented a comprehensive simulation of the SLS process, focusing on how laser parameters and scanning speeds influence microstructural features such as porosity, surface morphology, and densification. The study offers valuable insights into the thermal and microstructural dynamics during laser scanning in SLS.

### 2.3. Thermal Diffusion

Thermal diffusion distributes heat to adjacent particles, enhancing bonding without causing complete melting. This controlled heat transfer minimizes thermal stress and deformation, preserving dimensional accuracy.

As the laser moves away, the sintered material cools, solidifies, and crystallizes. These processes strengthen the part and improve dimensional stability. A thorough understanding of the melt pool's temperature distribution and dimensions is critical. Researchers have extensively studied melt pool dynamics through numerical simulations and experimental methods, focusing on energy density and process parameters.

Polivnikova [56] investigated thermal processes and melt pool behavior in both SLS and Selective Laser Melting (SLM). The study introduced models to analyze heat transfer, phase transitions, and the impact of process parameters on melt pool size and stability. The findings offer key insights into how controlled heat diffusion promotes particle bonding without full melting, reducing thermal stress and maintaining dimensional precision.

#### 2.4. Viscous Flow and Particle Coalescence

Viscous motion drives the consolidation of molten particles during sintering. The rate of coalescence is primarily influenced by zero-shear viscosity, which governs the fluidity of the polymer melt. Studies have shown that lower viscosity enhances fluidity, facilitating complete particle coalescence and consolidation.

Sintered particles form molecular bonds, creating a dense, uniform structure within and between layers. This process is repeated layer by layer to construct the final 3D object.

Benedetti *et al.* [57] studied how different Poly(aryl ether ketones) (PAEK) powders melt and merge. They tested three substrates: glass, silicone-coated glass, and amorphous PEKK films (relevant to laser sintering). They found that particles shrink by up to 30% before melting, then expand due to viscous flow. This shrinkage slows coalescence by pulling particles apart, explaining why neck growth is slower than expected. The substrate type had little effect, while viscosity and particle size played a bigger role in melting, with morphology and porosity having minimal impact.

#### 2.5. Solidification/Crystallization

Each layer formation concludes with cooling to the build temperature, which is higher than the polymer crystallization point.

Localized laser energy selectively melts the powder while the high melting enthalpy and low thermal conductivity of polymers prevent surrounding particles from melting. Understanding the interaction between solidifying powder and unmolten particles is essential, as these interactions affect the part's density, dimensional accuracy, and potential microstructural defects.

Soldner *et al.* [58] investigated the crystallization behavior of Polyamide 12 during SLS at a macroscopic scale using a finite element approach. To accurately capture the temperature fields inherent to SLS, they adapted the Nakamura model to account for a reduction in crystallization degree upon melting in an energetically consistent manner. Their study further demonstrated the influence of geometric dimensions on temperature distribution and crystallization dynamics, revealing that finer features cool much faster than larger ones, which directly affects the crystallization process.

#### 2.6. Post-processing

After the sintering process, any remaining unsintered powder is removed (and often recycled). The finished part may then undergo several post-processing steps. These can include heat treatment to reduce internal stress and improve its strength and other mechanical properties, as well as machining or polishing to enhance its surface finish and dimensional accuracy.

Agarwala *et al.* [59] provided an overview of post-processing techniques for selectively laser-sintered (SLS) metal parts aimed at enhancing structural integrity and inducing material transformations. The study presented findings on how liquid phase sintering temperature and duration affect material properties. Additionally, the authors described the hot isostatic pressing (HIP) process and its application to SLS metal parts, demonstrating its effectiveness in achieving near-full-density components.

In summary, the SLS process is a complex and highly controlled additive manufacturing technique that relies on precise powder spreading, laser irradiation, thermal diffusion, and particle coalescence to build high-quality 3D structures. Each stage, from powder preparation to post-processing, plays a crucial role in determining the final part's mechanical properties, dimensional accuracy, and surface finish. Advancements in material selection, process optimization, and computational modeling continue to enhance SLS capabilities, making it a valuable manufacturing method for diverse industrial applications.

### 3. Material Selection

Material selection in SLS is crucial for determining the final properties of printed parts. Polymers like nylon and polyamide are widely used due to their durability, flexibility, and suitability for functional prototypes and end-use parts. Recent advancements have enabled the processing of metals and metal-polymer composites. Composite powders, such as glass- or carbon-filled polymers, offer improved strength, stiffness, and thermal stability, making them ideal for demanding applications in automotive and aerospace. Each material's thermal and mechanical behavior affects sintering, layer adhesion, part density, surface finish, and mechanical properties, increasing SLS's versatility. Below are common SLS materials categorized by type.

#### 3.1. Polymers

##### 3.1.1. Nylon/PA 12

Nylon/PA 12 is a versatile material well-suited for SLS processing due to its strength, durability, and flexibility, making it ideal for parts that need to endure mechanical stress. Its high melting point ensures stability during the SLS process, producing parts with smooth surfaces, accurate dimensions, and excellent mechanical properties. PA 12's resistance to chemicals like oils, fuels, and solvents further enhances its suitability for demanding environments.

The material's low sensitivity to moisture facilitates easy storage and consistent processing, while its ability to form complex shapes and detailed designs makes it ideal for custom prototypes and small production runs. However, PA 12 can degrade under UV light, so UV protection is recommended for outdoor applications.

Fig. (3) [60] presents a micrograph of a sintered PA 12 part's cross-section, showing fused unmolten particles at the edge. The microstructure of the part consists of particle cores surrounded by spherulites. These cores represent unmolten regions of particles that did not receive enough heat to fully melt. Smaller particles, which fully melted during processing, formed spherulites without cores, highlighting the importance of precise thermal control during the SLS process.

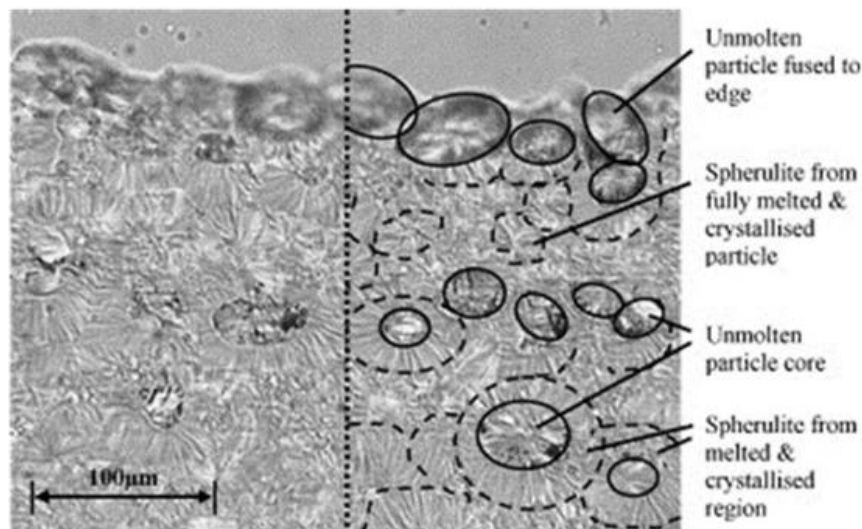


**Figure 3:** A cross-sectional optical micrograph of a sintered PA 12 part [60].

### 3.1.2. Nylon/PA 11

PA 11 is a durable material with excellent tensile strength, impact resistance, and flexibility, making it ideal for SLS-processed parts like automotive components, industrial tools, and aerospace applications. Its ability to absorb shocks and withstand pressure enhances its suitability for demanding environments.

With a melting point of 180–190°C, PA 11 performs well in the SLS process, maintaining its structure and quality. It resists oils, fuels, and solvents, and its low moisture absorption ensures consistent performance, even in humid conditions. Additionally, its renewable origin from castor oil makes it a more sustainable choice compared to petroleum-based nylons.

PA 11 powders flow and fuse efficiently during SLS, producing parts with smooth surfaces, precise dimensions, and excellent mechanical properties. The material supports the creation of complex designs that traditional methods cannot achieve. Proper handling and post-processing, such as heat treatment, can further optimize its properties.

Fig. (4) [61] presents a cross-sectional micrograph of an SLS-fabricated PA 11 part filled with 2% silica nanoparticles. The sample was dyed with black ink and wiped to highlight porosity. Black regions indicate pores where ink was retained, emphasizing the importance of process optimization to minimize porosity and achieve fully dense parts in SLS applications.

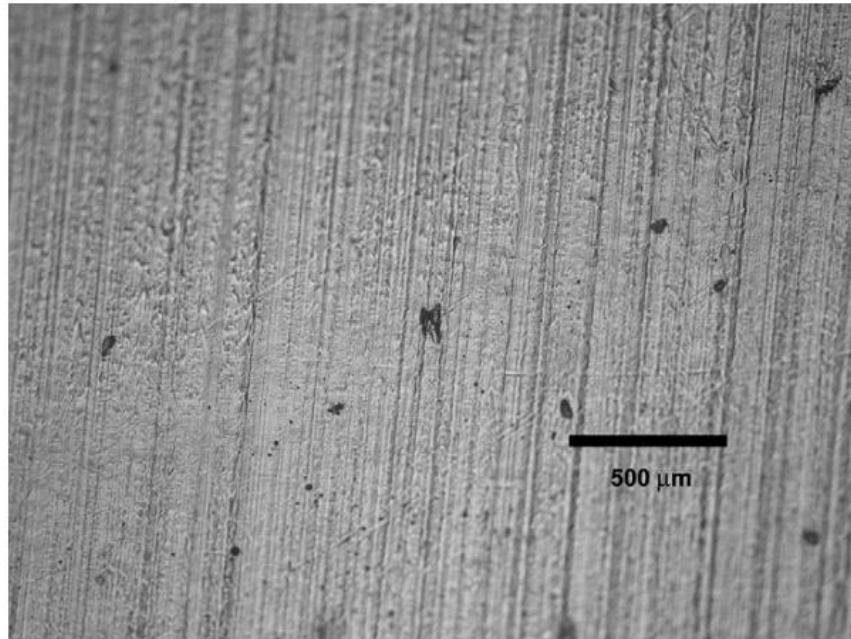


**Figure 4:** A cross-sectional optical micrograph of Nylon-11 + 2% silica nanoparticles [61].

### 3.1.3. Polypropylene (PP)

PP is a lightweight and durable material commonly used in automotive, packaging, and consumer products due to its strength and low weight. It resists chemicals like acids, alkalis, and solvents, making it suitable for harsh industrial environments. With a melting point of about 160°C, PP performs well during the SLS process, maintaining stability and quality.

During SLS, PP's flexibility and impact resistance allow it to absorb shocks without cracking, while its low moisture absorption ensures consistent performance, even in humid conditions. PP's powder form is stable and easy to handle, producing smooth and accurate parts. The SLS process also enables complex shapes and intricate features that traditional manufacturing cannot achieve. However, PP may not withstand extremely high temperatures or heavy stress as well as materials like polyamide (PA) or polycarbonate (PC).



Fig. (5) [62] highlights the surface characteristics of PP parts produced at various energy densities during SLS. At a low energy density of  $0.0138 \text{ MJ/m}^2$  (Fig. 5a), particles are loosely bonded with visible sintering necks, and individual particles remain distinct. As the energy density increases ( $0.0165$ – $0.0275 \text{ MJ/m}^2$ , Fig. 5b–d), more particles fuse together due to surface tension, forming a connected structure, though some unmelted particles are still visible (Fig. 5d). At higher energy densities (Fig. 5e–f), particle boundaries blur, and the surfaces become more compact. Despite the dense appearance at  $0.0458 \text{ MJ/m}^2$ , small pores less than  $1 \mu\text{m}$  in diameter remain detectable.

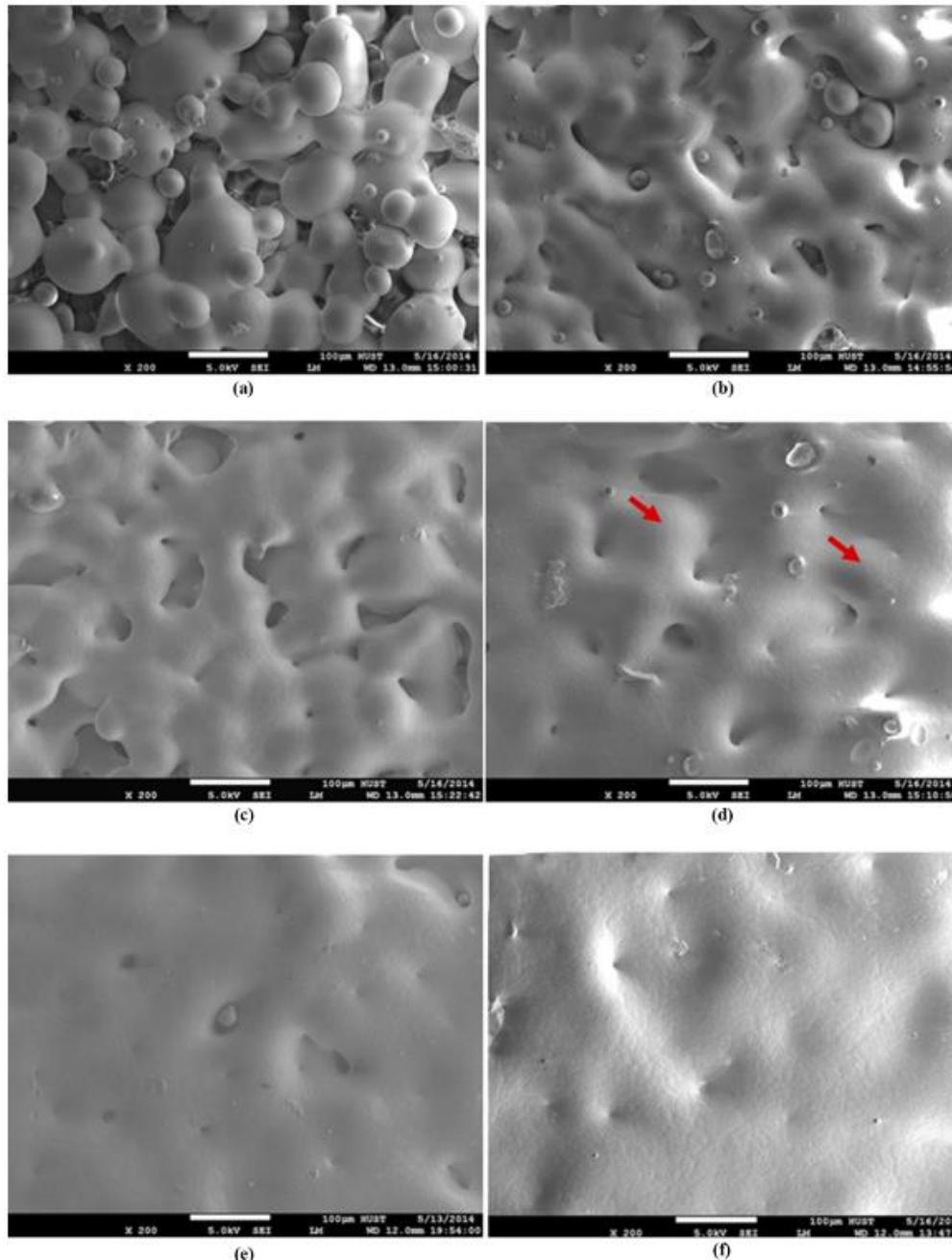


**Figure 5:** Morphologies of sintered PP specimens under energy densities: (a)  $0.0138$ ; (b)  $0.0165$ ; (c)  $0.0206$ ; (d)  $0.0275$ ; (e)  $0.0458$ ; and (f)  $0.055 \text{ MJ/m}^2$  [62].

### 3.1.4. Polyether Ether Ketone (PEEK)

PEEK is highly suitable for SLS processing due to its high melting point ( $343^\circ\text{C}$ ), allowing it to withstand the heat during sintering without degradation. PEEK powder flows smoothly and sinters efficiently, producing parts with

smooth surfaces and excellent mechanical properties. The SLS process enables the creation of complex designs and detailed internal features, making it ideal for customized and intricate parts with minimal post-processing.

Fig. (6) [63] illustrates the impact of sintering conditions on virgin and thermally aged PEEK powders. Single layers of virgin PEEK were successfully sintered at a laser power of 6 W in nitrogen or argon atmospheres (Fig. 6a and d). However, in air, the same conditions led to blackening and severe degradation, highlighting the importance of a protective gas during high-temperature sintering. Lower laser powers failed to melt the powders under these conditions. Fourier transform infrared spectroscopy (FTIR) analysis showed that PEEK powders aged in air decomposed significantly, making them difficult to sinter at 330°C due to partial decomposition. This emphasizes that PEEK powders exposed to oxygen-containing atmospheres cannot be reused effectively.

Adjustments to laser power helped mitigate these issues. For aged powders (e.g., Ar2/N2, Ar4/N4, and Ar8/N8), sintering was successful at reduced laser powers of 5.5, 5, and 4 W, respectively, producing smooth sintered surfaces (Fig. 6b, e, h, k). High magnification revealed distinct crystal boundaries in virgin PEEK samples (Fig. 6c and f), while these were less noticeable in aged samples sintered in argon or nitrogen (Fig. 6i and l). However, micro density measurements indicated that aged samples (Ar8 and N8) had lower densities compared to virgin PEEK.

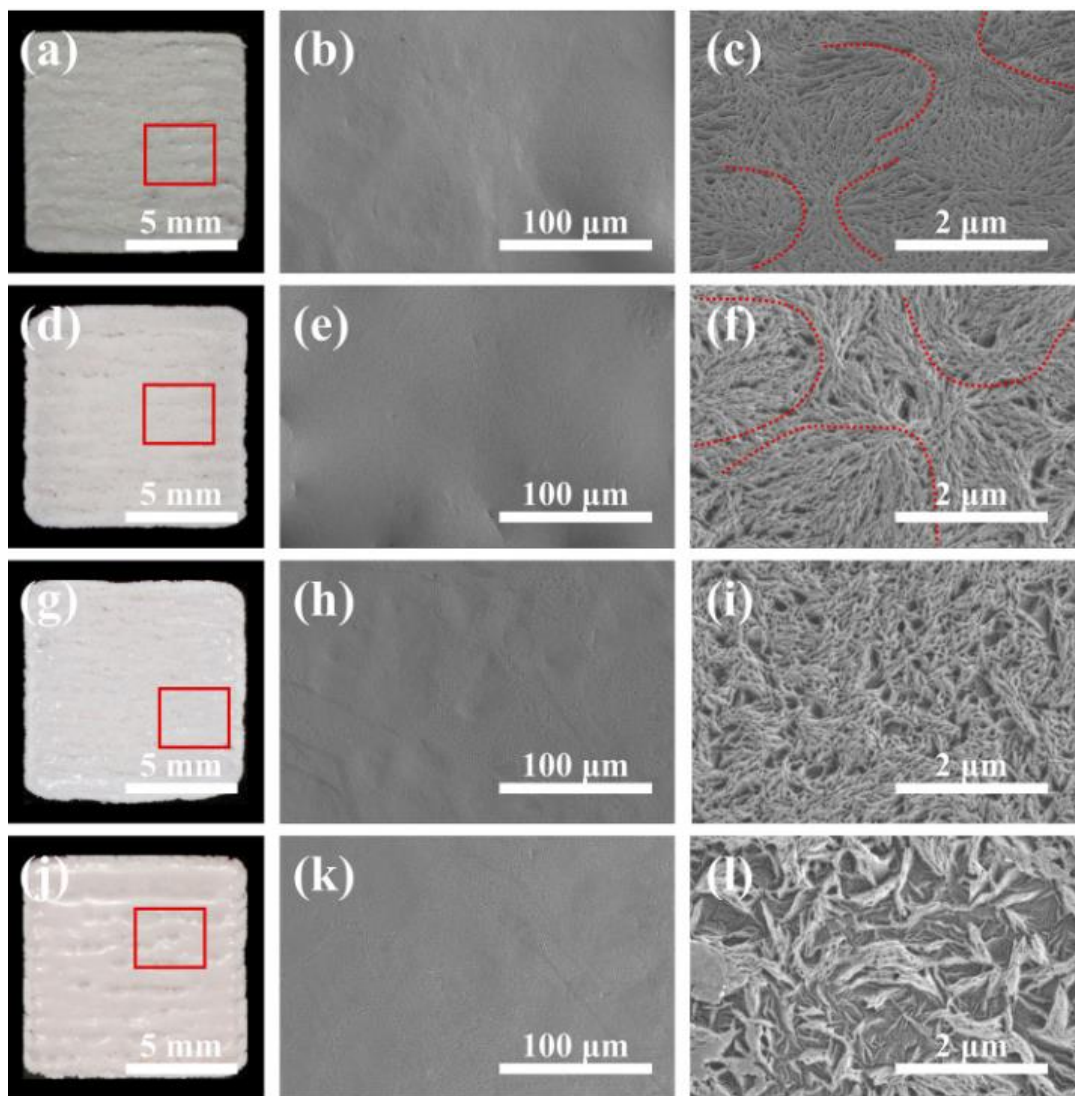


**Figure 6:** Single-layers and SEM images of virgin PEEK powders sintered in (a-c) argon and (d-f) nitrogen; (g-h) thermally aged Ar8 powders sintered in argon, and (i-l) thermally aged N8 powders sintered in nitrogen, respectively. Arcs indicate the crystal boundaries [63].

### 3.1.5. Thermoplastic Polyurethane (TPU)

TPU is well-suited for SLS processing, particularly for creating flexible, elastic, or shock-absorbing parts. Its stretchability and durability make it ideal for complex designs, including internal features and flexible joints, which are difficult to achieve with traditional methods. TPU's versatility in hardness levels allows for both soft and rigid components. Additionally, SLS processing requires minimal post-processing for TPU parts, making it a cost-effective choice for rapid prototyping and small-batch production.

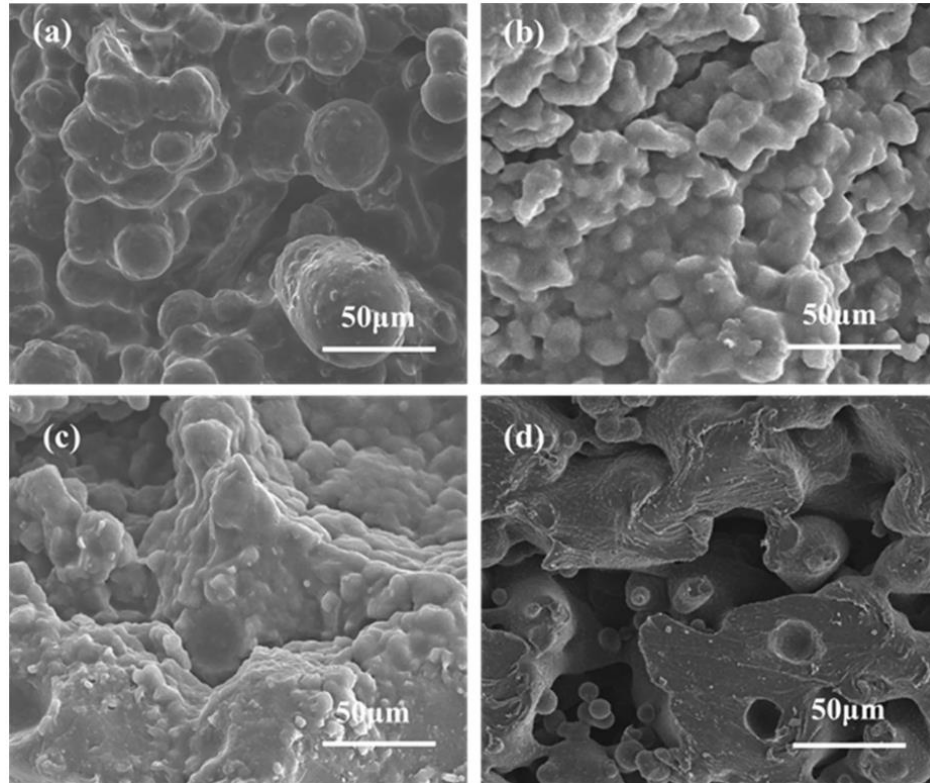


**Figure 7:** SEM images of TPU powder sintered at different laser powers: (a) 20 W, (b) 30 W, (c) 40 W, and (d) 50 W [64].

Fig. (7) [64] highlights the impact of laser energy density (ED) during the TPU SLS process. At high laser ED (Fig. 7d), issues like the formation of "balls" occur near the molten powder, disrupting the creation of smooth, uniform layers. These balls hinder the even spreading of new powder over previously sintered layers, leading to defects such as cracks, porosity, and rough surfaces. Excessive laser energy also causes partial powder degradation, generating gas that forms additional pores, further weakening mechanical properties.

## 3.2. Metals

### 3.2.1. Stainless Steel

Stainless steel, particularly grades like 316L and 17-4PH, is highly suitable for SLS processing due to its strength, corrosion resistance, and performance in demanding applications. The spherical powder, created through gas or plasma atomization, flows smoothly during printing, ensuring dense and high-quality parts. Its moderate melting temperature aligns well with SLS laser energy, enabling efficient sintering or melting with minimal thermal stress.

Printed stainless steel parts are durable, with properties that can be enhanced through post-processing like heat treatment. Fig. (8) [65] shows that sintering temperature significantly affects pore characteristics in 316L stainless steel. At lower temperatures (1100°C), pores are interconnected with an average size of 160 μm. As the temperature increases, pore size decreases, and most pores close completely at 1300°C, resulting in more compact parts. This adaptability makes stainless steel ideal for producing durable, high-performance components with SLS.

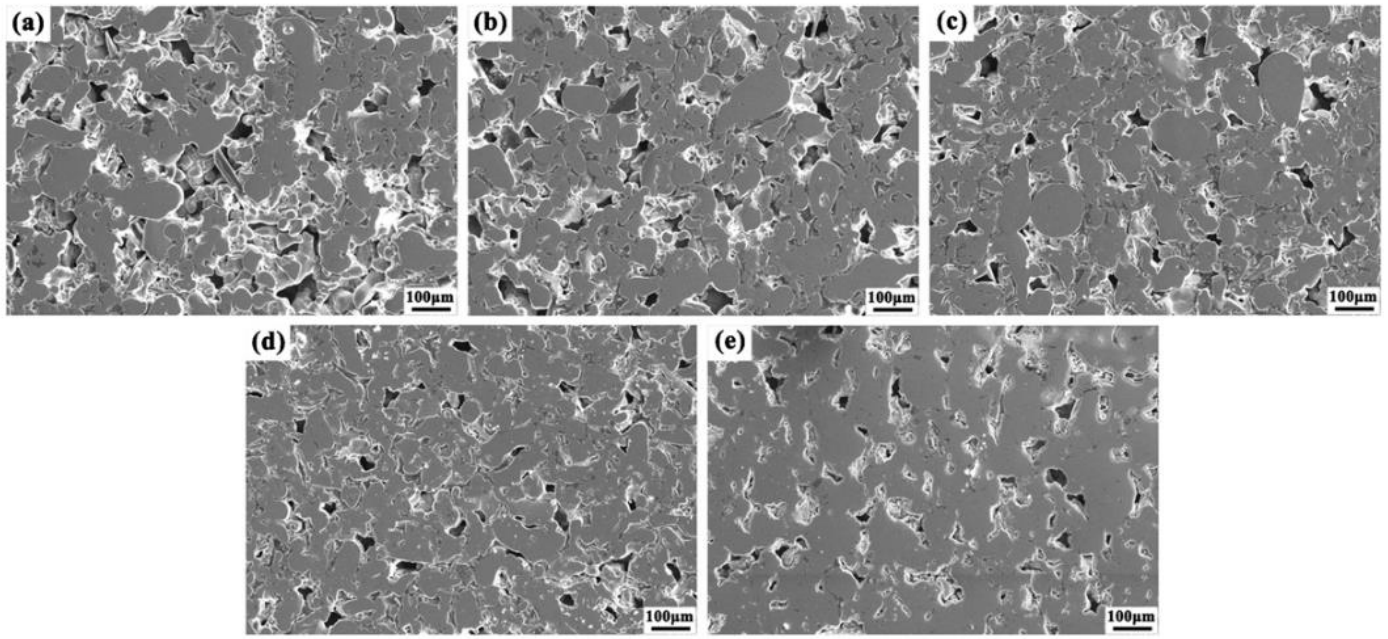


**Figure 8:** SEM images of porous 316L SS sintered at various temperatures: (a) 1100 °C; (b) 1150 °C; (c) 1200 °C; (d) 1250 °C; (e) 1300 °C [65].

### 3.2.2. Aluminum

Aluminum, particularly alloys like AlSi10Mg and Al6061, is well-suited for SLS processing due to its high strength-to-weight ratio and excellent thermal and electrical conductivity. Gas-atomized aluminum powders form spherical particles that flow smoothly and distribute evenly during printing, ensuring consistent and high-quality results. The material works efficiently with high-energy SLS lasers, enabling precise sintering. Post-processing options, such as heat treatment or anodizing, can enhance aluminum parts' strength and surface finish.

Fig. (9) [66] illustrates the microstructural changes with varying laser energy intensities. At a high energy density (100 J/mm<sup>3</sup>), slower cooling leads to coarser dendritic structures and some irregularly shaped pores surrounded by a dense aluminum-silicon matrix. Reducing the energy density to 67 J/mm<sup>3</sup> results in faster cooling and a finer microstructure, demonstrating how energy input affects the quality of aluminum parts in SLS.

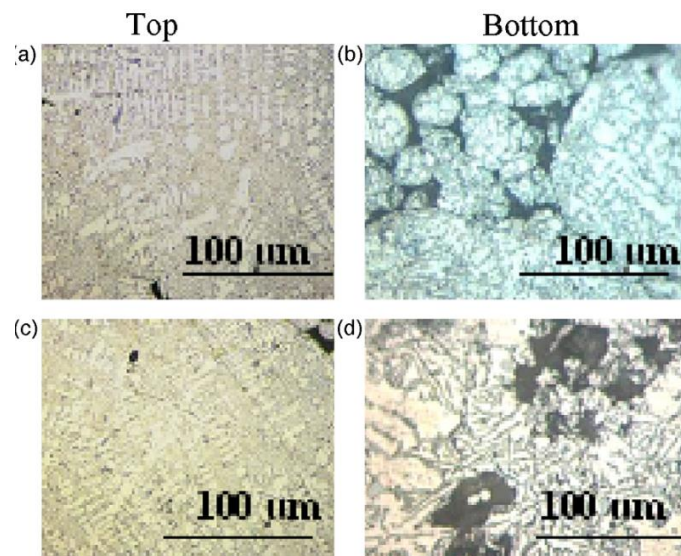


**Figure 9:** Characteristic microstructures of SLS processed AlSi12 powder with varying laser intensities: (a and b) 100 J/mm<sup>3</sup>; (c and d) 67 J/mm<sup>3</sup> [66].

### 3.2.3. Titanium

Titanium alloys, such as Ti-6Al-4V, are excellent for SLS processing due to their high melting point (~1,668°C) and ability to produce dense, mechanically robust parts. High-powered lasers precisely melt and solidify titanium powders, ensuring dimensional accuracy and quality. The powders, typically gas-atomized into spherical particles, offer smooth flow and uniform layer spreading, which are essential for the SLS process.

SLS experiments on titanium powders using pulsed and continuous wave laser modes are illustrated in Fig. (10) [67]. Fig. (10a) shows an optical micrograph of the titanium powder bed surface after continuous wave sintering. The laser scan strategy creates visible separation lines. During continuous wave sintering, the powder grains are evenly heated, resembling a “cooking” process, with no significant difference between the peak and average temperatures. The micrograph reveals a combination of solid-state sintering, where individual grains remain intact (melting temperature not reached), and liquid-phase sintering, seen as light tracks where melting occurs. Melting happens only in areas where the temperature exceeds titanium’s melting point of 1660°C.

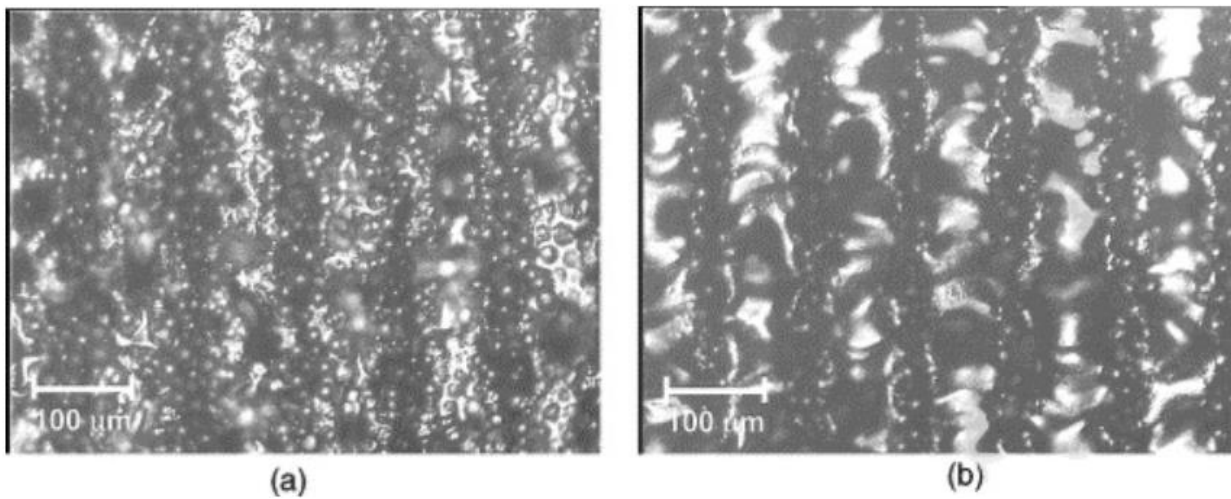


**Figure 10:** Optical micrographs of titanium sintered by (a) continuous wave laser (3 W average power) and (b) pulsed laser (2 W average power) [67].

### 3.2.4. Cobalt-Chromium (Co-Cr) Alloys

Co-Cr alloys are well-suited for SLS processing due to their high melting point (1,300–1,500°C), which aligns with high-powered laser capabilities, enabling precise melting and fusion of powder layers. Gas-atomized Co-Cr powders with spherical particles ensure smooth flow and uniform layer spreading, resulting in dense, high-quality prints.

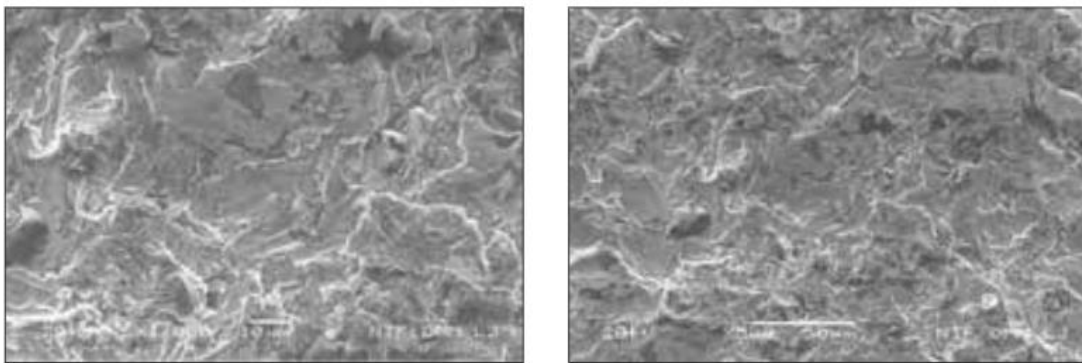


**Figure 11:** Micrographs of Co-Cr Alloy Surfaces: (a) Sintered and Thermally Treated; (b) Sintered, Thermally Treated, and Sandblasted [68].

SLS-produced Co-Cr alloy parts have a more uniform structure but exhibit slight porosity compared to cast alloys, as shown in Fig. (11) [68]. Post-processing, such as heat treatment and polishing, improves mechanical properties and surface finish, making these alloys ideal for medical implants, dental restorations, and aerospace applications.

### 3.2.5. Tool Steel

Tool steels like Maraging Steel, H13 Tool Steel, and A2/D2 steels are excellent for SLS due to their hardness, wear resistance, and thermal stability, enabling them to withstand the high temperatures and stresses of the process. Gas-atomized tool steel powders with spherical particles ensure smooth flow and uniform layer spreading, critical for achieving consistent density and precise geometries. Their melting points (1,300–1,500°C) are compatible with SLS's high-energy lasers, allowing precise melting and fusion for dense, uniform microstructures.

SLS-produced tool steel parts benefit from post-processing, such as heat treatment and machining, to enhance hardness and toughness for specific applications. Precise laser parameters during SLS influence microstructure, with rapid cooling contributing to martensitic transformations and carbide formations. These characteristics make tool steels ideal for functional prototypes, injection molds, and components in industries like aerospace and automotive.

Fig. (12) [69] shows how different laser systems affect microstructures in SLS. The Nd: YAG laser produces fine, dendritic cellular grains with a martensitic matrix, while the CO<sub>2</sub> laser creates similar structures with chromium-rich regions due to reheating. Rapid cooling after reheating leads to unique microstructures with martensitic transformations and carbide formations, highlighting how precise laser parameters control the properties of tool steel parts in SLS.

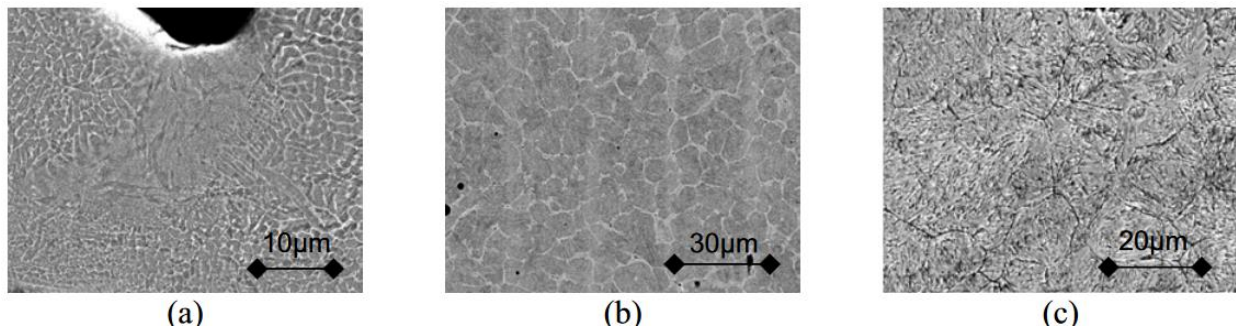


**Figure 12:** Micrographs of H13 powders scanned by (a) Nd: YAG laser [Pulsed Mode], (b) and (c) CW CO<sub>2</sub> laser [69].

## 3.3. Ceramics

### 3.3.1. Alumina (Aluminum Oxide)

Alumina is ideal for SLS due to its hardness, high melting point (~2,072°C), and excellent thermal and chemical properties, making it suitable for wear-resistant tools, heat exchangers, electronic substrates, and medical implants. Its biocompatibility and dielectric strength expand its use in advanced applications.

Spherical alumina powder with controlled particle size ensures smooth flow, even layer distribution, and consistent sintering. High-powered lasers bond particles effectively, allowing the creation of intricate geometries that are difficult to achieve with traditional methods. This results in lightweight, durable components with superior mechanical and thermal performance.

SLS processing of alumina produces sintered parts with a porous network of densified microspheres, achieving a density of 1.50 g/cm<sup>3</sup> (38.5% of alumina's theoretical density). These parts feature large, isolated pores and a density gradient between the core and edges, as shown in Fig. (13) [70]. This combination of properties makes alumina ideal for high-precision, high-performance applications.

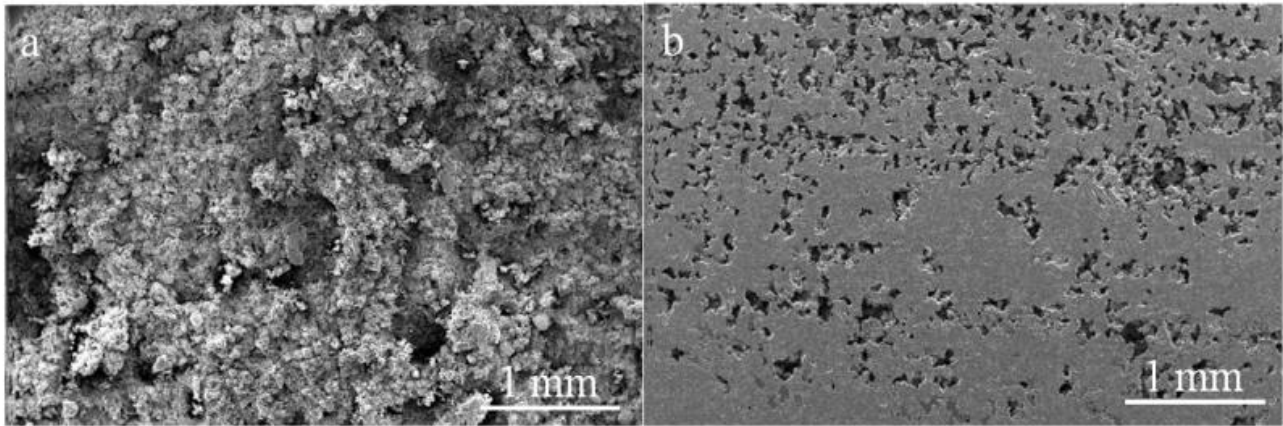


**Figure 13:** Micrographs of cross-sections of sintered alumina produced by SLS [70].

### 3.3.2. Silicon Carbide (SiC)

Silicon Carbide (SiC), with its high melting point ( $\sim 2,700^{\circ}\text{C}$ ) and excellent thermal stability, is well-suited for the extreme conditions of the SLS process. The laser selectively sinters the powder without degrading its material properties, preserving SiC's inherent strengths.

SiC's high thermal conductivity ensures efficient heat dissipation during sintering, reducing thermal stresses and warping in printed parts. Its resistance to oxidation and chemical reactions makes it ideal for chemically demanding environments. SLS enables precise control over the densification of SiC parts, allowing the production of components with tailored porosity, density, and microstructure, essential for applications like heat exchangers, filters, and structural components.

Due to SiC's resistance to melting, indirect SLS is often used, where a polymer binder or reactive additive is mixed with the SiC powder to assist in sintering. Fully densified parts typically undergo post-sintering or infiltration to enhance mechanical and thermal properties.

As shown in Fig. (14) [71], SEM images reveal scanning paths following a zigzag strategy (inclined at  $45^{\circ}$ ). The surface is smooth, with visible porosity and sintered particles, confirming the feasibility of direct scanning for SiC and similar ceramics without requiring a melting phase.

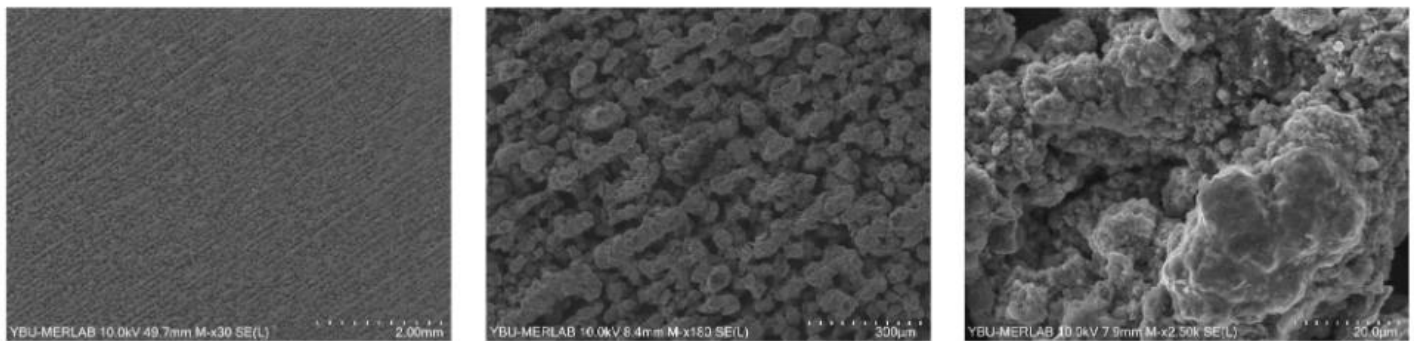


**Figure 14:** SEM images of SiC samples printed at a high laser energy density [71].

### 3.3.3. Zirconium Dioxide ( $\text{ZrO}_2$ )

Zirconium Dioxide ( $\text{ZrO}_2$ ), or zirconia, is well-suited for SLS due to its durability, high strength, and crack resistance, making it ideal for applications such as dental crowns and medical implants. Its high melting point ( $\sim 2,700^{\circ}\text{C}$ ) allows it to withstand the elevated temperatures required for SLS sintering.

Zirconia's low thermal conductivity helps retain heat during printing, reducing thermal stress and enabling efficient laser fusion. Its resistance to oxidation, corrosion, and chemicals makes it suitable for demanding environments like aerospace and chemical processing.

Spherical zirconia powders ensure smooth flow and uniform layer spreading, which supports consistent part quality. The SLS process enables precise control over density and porosity, allowing to produce tailored components. By managing phase changes during sintering, zirconia's toughness can be enhanced, though careful processing is required to avoid cracks or unwanted phase transitions. Post-sintering processes may be necessary to achieve optimal strength and performance.

As shown in Fig. (15) [72], the microstructure of as-SLS zirconia consists of joined powder microspheres with inter-agglomerate voids due to limited plastic flow during sintering (Fig. 15a). Warm isostatic pressing (WIPing) improves this, resulting in a more homogeneous microstructure and higher density through plastic deformation (Fig. 15b and c).

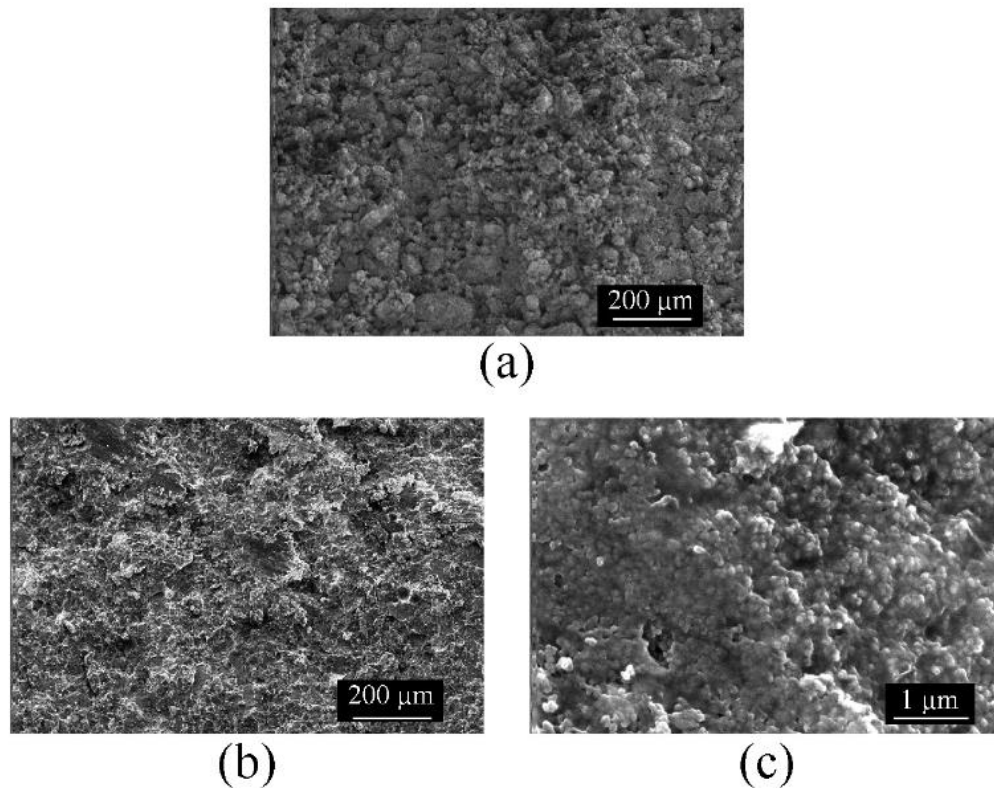


**Figure 15:** Micrographs of zirconia samples produced by (a) SLS and (b, c) SLS + WIP [72].

#### 3.3.4. Hydroxyapatite (HA)

Hydroxyapatite (HA) is highly biocompatible, making it ideal for medical implants, dental applications, and bone scaffolds. As a primary component of bone, HA supports bone growth, crucial for orthopedic and dental uses.

SLS enables precise control over HA's porosity and structure, allowing the production of scaffolds that closely mimic natural bone and promote cell growth and tissue regeneration. HA can withstand the high temperatures (~1500–1600°C) used in SLS without degrading. Additionally, it can be combined with polymers to improve strength and printability while maintaining biocompatibility.

Detailed and custom HA structures can be created using SLS for applications in regenerative medicine. However, careful sintering is required to prevent cracking or shrinkage. Post-sintering processes like coating or densification are often necessary to enhance durability and bioactivity.



Laser energy density significantly impacts the quality of sintered HA parts. As shown in Fig. (16) [73], at a low energy density ( $2.0 \text{ J/mm}^2$ ), powders are slightly fused, resulting in many connective pores (Fig. 16A). At  $3.0 \text{ J/mm}^2$ , a well-defined layer structure forms with fewer pores (Fig. 16B). At  $4.0 \text{ J/mm}^2$ , densification is nearly complete with minimal porosity (Fig. 16C). However, at  $5.0 \text{ J/mm}^2$ , excessive energy causes decomposition, resulting in large pores and reduced density (Fig. 16D). This highlights the need for optimized energy settings to achieve high-quality HA components.

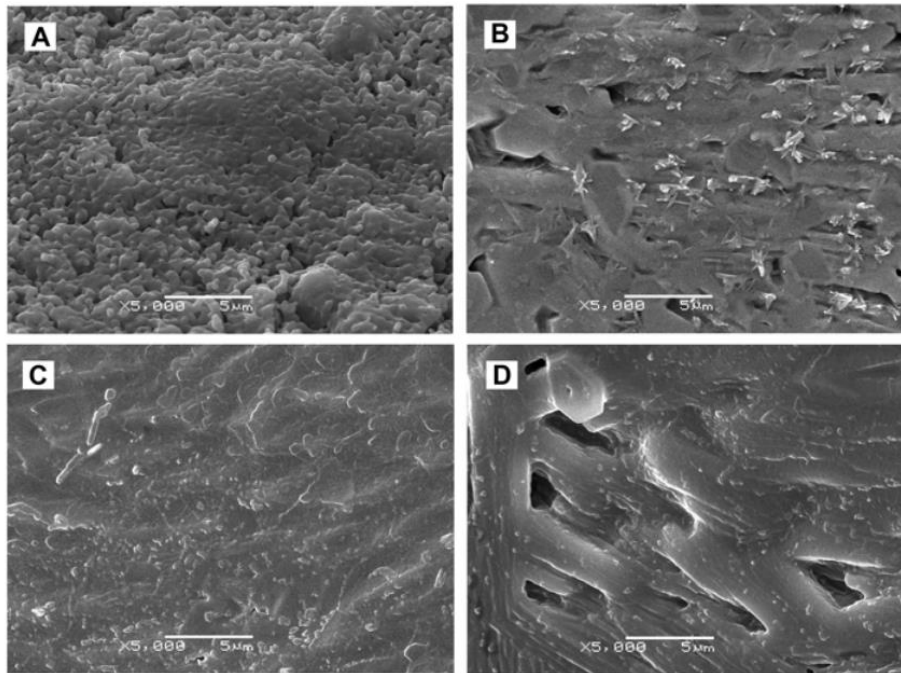


**Figure 16:** Micrographs of the HA samples at different laser energy densities: (A)  $2.0 \text{ J/mm}^2$ ; (B)  $3.0 \text{ J/mm}^2$ ; (C)  $4.0 \text{ J/mm}^2$ ; and (D)  $5.0 \text{ J/mm}^2$  [73].

In summary, material selection is crucial in SLS, as it directly affects the final properties of printed parts. Common materials include polymers, metals, and ceramics, each offering distinct advantages. Polymers like Nylon/PA 12 and PA 11 provide strength, flexibility, and chemical resistance, with PA 12 ensuring smooth surfaces and dimensional accuracy, while PA 11 offers better impact resistance and sustainability. Polypropylene (PP) is another lightweight option valued for its chemical resistance. Metals such as stainless steel, aluminum, and titanium are ideal for high-strength applications, with stainless steel offering durability and corrosion resistance, aluminum providing lightweight thermal conductivity, and titanium delivering exceptional mechanical strength for aerospace and medical uses. Ceramics, including alumina, silicon carbide (SiC), and hydroxyapatite (HA), support applications requiring high thermal stability, wear resistance, and biocompatibility, with alumina used in heat exchangers and implants, SiC excelling in extreme environments, and HA being essential for bone scaffolds in regenerative medicine. The thermal and mechanical behavior of each material influences sintering, adhesion, density, and surface finish, making material selection a key factor in optimizing SLS for diverse applications.

## 4. Process Parameters and Optimization

In SLS, key process parameters, shown in Fig. (17), significantly affect the quality, accuracy, and mechanical properties of the final parts. Laser power controls the energy delivered to the powder bed; insufficient power results in poor sintering, while excessive power can cause overheating and distortion. Scan speed influences heat distribution and layer bonding by affecting the laser's dwell time. Other factors, such as layer thickness, impact build time and resolution, while hatch spacing determines the overlap between laser scans. Optimizing these parameters [74] improves part density, reduces porosity, and enhances mechanical properties, ensuring high-quality, reliable parts for various applications.

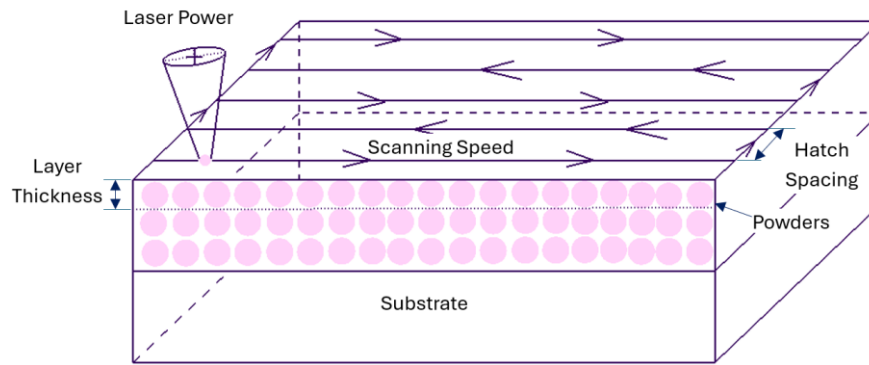


**Figure 17:** SLS process parameters.

#### 4.1. Laser Power

Laser power plays a crucial role in determining the quality and performance of a final product. Higher laser power improves sintering efficiency, leading to denser, stronger parts with smoother surfaces and better dimensional accuracy [75-77]. Gharate *et al.* [75] studied the impact of laser power ratios (LPRs) on sintering in SLS. They tested mixtures of Kollidon SR (98.75%) and an IR-absorbing dye (1.25%) for particle size and flowability. Higher LPRs improved sintering, with the best accuracy and yield at an LPR of 3.0. SEM analysis revealed the internal structure of the prints. Vande Ryse *et al.* [76] examined how SLS parameters (laser power, bed temperature, and layer thickness) affect a thermoplastic elastomer polyester. They found that using 17–20 W laser power improved density, mechanical properties, and reduced yellowing. They also proposed improved equations and guidelines for predicting laser power and temperature effects. Kozak and Zakrzewski [77] developed a thermal model describing laser heating, melting, and solidification of powder layers. Their sensitivity analysis showed how changes in laser power, spot size, exposure time, and powder properties influence the size of the melted track.

However, excessive laser power can cause rough surfaces, heat stress, and defects. Bian *et al.* [78] investigated how laser power and scanning strategies affect residual stress in 316L steel during selective laser melting (SLM). Using both simulations and experiments, they tested four conditions: two laser power levels (160 W and 200 W) and two scanning strategies (stripe and chessboard). In all cases, residual stress increased with depth. Higher laser power (200 W) and stripe scanning led to greater residual stress, with laser power having a more significant effect than scanning strategy.

#### 4.2. Scanning Speed

Scanning speed, or how fast the laser moves across the powder bed, is crucial in SLS as it impacts the final product's quality. Faster scanning can create smoother surfaces but may weaken the part and reduce adhesion. Slower speeds can cause overheating, leading to pores and weak spots [79, 80]. Hou *et al.* [79] studied the effects of laser power and scanning speed on dimensional accuracy using PA2200 powder. They found the optimal settings: 40 W laser power and 5000 mm/s scan speed, resulting in dimensional deviations of -0.35% (X), -0.4% (Y), and -0.25% (Z). Jain *et al.* [80] examined how process parameters like layer thickness, energy density (a combination of laser power, beam speed, and hatch spacing), bed temperature, and hatch pattern influence part strength. Using the Taguchi method with an L16 modified orthogonal array, they fabricated polyamide (PA2200) tensile specimens following ASTM D638 standards. The specimens were tested for tensile strength using a universal testing machine. By maximizing the signal-to-noise (S/N) ratio and using ANOVA, they identified the most influential parameters. A regression model was developed to predict part strength, and confirmation tests showed results within the confidence interval.

#### 4.3. Layer Thickness

Layer thickness affects part quality and build speed. Thicker layers speed up printing but create rougher surfaces, higher thermal stress, and defects like warping or cracking. They also lower part density and increase

porosity, weakening strength and stiffness. Thinner layers improve surface finish, resolution, and accuracy but take longer to build, increasing costs. Chatterjee *et al.* [81] studied SLS of low-carbon steel powder using a pulsed Nd: YAG laser (100W max). They examined how layer thickness and hatching distance impact density, hardness, and porosity. Their experiments showed that increasing these parameters raised porosity, reducing hardness and density.

#### 4.4. Hatch Spacing

Hatch spacing, the distance between adjacent laser scan lines, is a critical parameter in SLS that significantly affects the quality and properties of the final product. Smaller hatch spacing results in a denser, more solid part with improved mechanical properties and a finer surface finish. Additionally, smaller hatch spacing can lead to improved dimensional accuracy. However, smaller hatch spacing requires more laser passes, which can significantly increase build time. Larger hatch spacing, on the other hand, can reduce build time but can result in lower part density, reduced mechanical properties, and a coarser surface finish. Danezan *et al.* [82] studied how laser energy density (controlled by laser power and scan speed) and hatching space affect SLS. They found that an energy density of 180–280 J/cm<sup>2</sup> with a hatching space above 30 μm produced strong, well-densified 3D objects. However, higher energy densities or smaller hatching spaces caused excessive melting of the material.

#### 4.5. Preheating Temperature

Preheating the powders before the build process can improve sintering by raising the starting temperature of the particles. This helps increase part density, reduce porosity, and enhance mechanical properties. Preheating also minimizes thermal gradients and residual stress, lowering the risk of distortion or cracking. However, it increases energy consumption and may accelerate material degradation, especially for temperature-sensitive materials. Li and Dong [83] analyzed how temperature control in the SLS process of PSB powders affects part precision through orthogonal experiments and variance analysis. Their results showed that different preheating stages impact precision in various ways. The preheating temperature before the first layer significantly affects warping, while the temperature before the last layer influences dimensional variation. The optimal temperature settings were 85°C for the initial preheating phase (TA), 105°C before sintering the first layer (TB), and 85°C before the last layer (TC).

#### 4.6. Part Bed Temperature (T<sub>b</sub>)

The temperature of the powder bed during the SLS process significantly influences the sintering process and the resulting part properties. A higher bed temperature can enhance sintering efficiency, leading to improved part density, mechanical properties, and surface finish. Additionally, a higher bed temperature can reduce thermal gradients within the part, minimizing the risk of part distortion or cracking. However, higher bed temperatures can increase energy consumption and may accelerate material degradation, particularly for temperature-sensitive materials [84]. Sachdeva *et al.* [84] studied the surface roughness of DuraForm polyamide parts made with SLS. They developed models to predict how factors including part bed temperature affect surface roughness. The factors were optimized and tested through experiments. Results showed that as the bed temperature increased from 172°C to 178°C, surface roughness first improved and then worsened. In laser sintering, the crystallization rate impacts curling, accuracy, and surface finish, with slower recrystallization at lower temperatures being beneficial. Low *et al.* [85] examined how bed temperature affects the porosity of cylindrical disc matrices used in drug delivery. They tested temperatures from 140°C to 155°C in 5°C steps, building samples in different orientations. After cleaning and drying, porosity was measured with a mercury porosimeter. Results showed an inverse linear relationship between bed temperature and porosity.

#### 4.7. Powder Morphology

Powder morphology refers to the shape, size, and surface features of powder particles. Particle shape and size affect powder flowability, packing density, and sintering behavior. Spherical particles tend to pack more efficiently, leading to higher part density and improved mechanical properties. Irregular particles, while less efficient in packing, can fill gaps between spherical particles, potentially improving overall packing density. A mix of particle

sizes can optimize packing density and sintering performance. Additionally, particle surface area can influence sintering kinetics. Higher surface area can accelerate sintering but may also increase the risk of porosity formation if not controlled. Sofia *et al.* [86] explored the feasibility of conducting SLS using powder mixtures composed of particles of varying sizes. Microphotographic analysis of the sintered specimens revealed that the mechanical strength of the material is highly dependent on the proportion of fine particles in the mixture, despite minimal effects on specimen thickness and density. Notably, the highest material strength was observed in specimens with the greatest fraction of fine particles. Simulation results indicated that, under the given process conditions, the bonding between large and fine particles was significantly weaker than that between particles of similar size. Additionally, the simulations suggested that the strength of sintered materials from mixed powders could potentially exceed that of materials sintered from unimodal powder components.

#### 4.8. Process Optimization

SLS involves many variables, such as laser power, scan speed, hatch spacing, and powder bed temperature, which affect part quality. Optimizing these factors is challenging due to their complex interactions. Czelusniak and Amorim [87] used Gaussian process machine learning to analyze how laser settings influence the quality of carbon fiber-reinforced PA12 parts and applied optimization techniques to identify the best settings for different objectives. Their results highlighted the significant impact of laser settings on part properties. Similarly, Abdelmoula *et al.* [88] also developed a numerical model to optimize process parameters for direct SLS (D-SLS) of SiC. Guided by the model, they successfully printed SiC samples, confirming its reliability.

The quality, accuracy, and mechanical properties of SLS-fabricated parts depend on key process parameters. Laser power controls energy input, affecting sintering efficiency and part density; while higher power improves strength and accuracy, excessive power can cause defects and residual stress. Scanning speed influences heat distribution and bonding, with faster speeds enhancing surface smoothness but weakening adhesion, while slower speeds risk overheating and porosity. Layer thickness impacts resolution and build time—thicker layers speed up production but increase porosity, whereas thinner layers enhance accuracy at the cost of longer processing. Hatch spacing determines scan line overlap, where smaller spacing improves strength but extends build time. Higher preheating and bed temperatures reduce porosity and thermal stress but raise energy consumption and risk material degradation. Powder morphology also plays a crucial role, as fine particles enhance strength, though irregular shapes may reduce flowability. Optimizing these parameters ensures the production of high-quality, reliable SLS parts for various applications.

## 5. Challenges and Limitations

SLS faces several challenges that impact the quality, efficiency, and scalability of the process. Fig. (18) illustrates the key challenges in SLS, emphasizing the importance of overcoming these obstacles to enhance the process and expand its use across various industries.

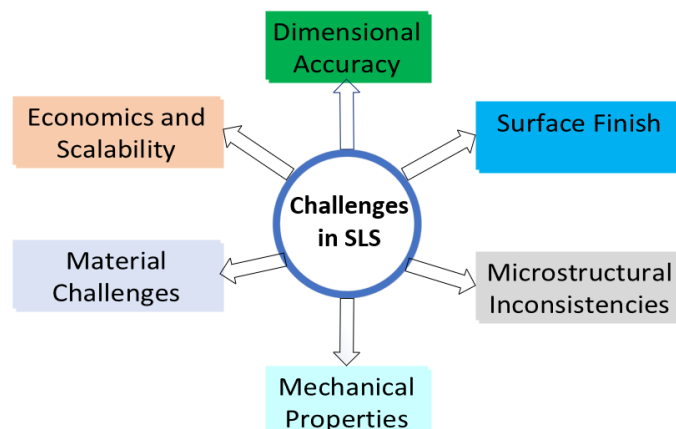


**Figure 18:** Challenges in SLS.

### 5.1. Dimensional Accuracy

Dimensional inaccuracies in SLS parts result from factors such as thermal shrinkage, uneven powder distribution, and the staircase effect on curved surfaces, leading to deviations from the intended design, especially along the Z-axis. Warping and distortion are often caused by residual stress from rapid heating and cooling cycles. Mitigation strategies include optimizing build orientation, refining process parameters, and applying compensatory design adjustments. Singh *et al.* [89] found that polyamide powder expands during sintering, which affects powder spreading and dimensional accuracy, with a maximum error of 0.192%. This expansion is primarily due to the powder's high linear expansion ratio.

### 5.2. Surface Finish

SLS parts often have rough surfaces due to the powder-based process and layer-by-layer construction. Smoother finishes typically require post-processing, such as sanding, polishing, or chemical treatments, which can be time-consuming and challenging to automate, especially for complex shapes. Beard *et al.* [90] used a Raman spectroscopy to study surface roughness under different process conditions. Figs. (19) and (20) show that increasing scan speed leads to higher surface finish, as particles have less time to consolidate.

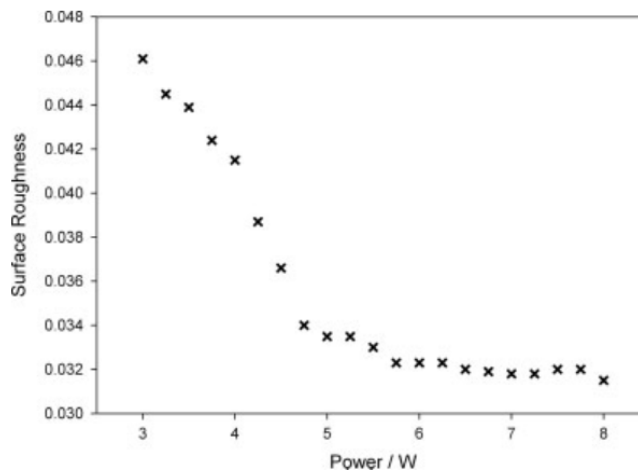


**Figure 19:** Surface roughness of sintered samples manufactured at a scan speed of 1200 mm s<sup>-1</sup> as a function of laser power.

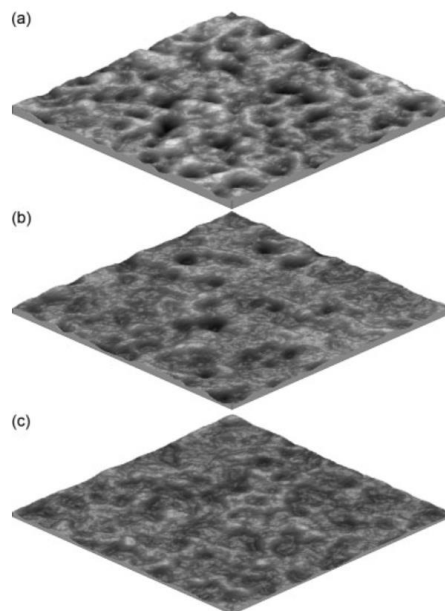


**Figure 20:** 3D surface profile of sintered components at 1200 mm/s scan speed with laser powers: (a) 3 W, (b) 4.5 W and (c) 8 W.

### 5.3. Microstructural Inconsistencies

The microstructure of SLS parts is typically heterogeneous, anisotropic, and porous, influenced by factors like scan patterns, energy density, bed temperature, and solidification conditions. Preheating the powder bed and optimizing scan parameters can reduce inconsistencies, but achieving uniformity is still challenging. High porosity weakens mechanical strength and durability, requiring extensive testing and refinement. Salmoria *et al.* [91] investigated SLS parts made from polyamide 6 (PA6) and polyamide 12 (PA12) blends, finding that powder properties, blend composition, and processing parameters affected the microstructure. During sintering, polyamides absorbed laser energy to melt the polymer phases. The resulting microstructures were heterogeneous, with co-continuous or dispersed phases depending on the PA12 content, and porosity and crystallinity varied with the blend ratio.

### 5.4. Mechanical Properties

Residual stresses and structural flaws resulting from rapid thermal cycling can compromise the mechanical integrity of SLS parts. Thermal gradients during printing contribute to internal stresses, potentially causing cracks or distortions in large or intricate geometries. Heat treatments such as annealing can help alleviate these stresses but add time and cost to production. Balan *et al.* [92] evaluated the effects of post-heat treatment on SLS-printed specimens using mechanical testing and microscopic analysis. Heat treatment significantly improved the mechanical properties of SLS parts, resulting in an average tensile strength of 28.06 MPa, a surface roughness of 2.4  $\mu\text{m}$ , a Shore D hardness of 49.48, and a specific wear rate of  $17.49 \times 10^{-5}$  kg/Nm. Compared to untreated parts, tensile strength and hardness increased by 6.5%, while surface roughness and wear rate were reduced by 51.67% and 50.3%, respectively. These results demonstrate that heat treatment greatly enhances the mechanical performance of SLS-printed components.

### 5.5. Material Challenges

Not all materials are suitable for the SLS process, as material selection poses challenges related to sintering behavior, thermal stability, and post-processing compatibility. Powders prone to contamination require meticulous handling to maintain performance, while recycling excess powder can reduce waste but risks quality degradation with excessive reuse. Toncheva *et al.* [93] addressed these challenges by incorporating recycled tire rubber into polymer matrices for SLS, blending up to 40 wt.% tire powder with polyamide and thermoplastic polyurethane to create composites with improved properties. Patel *et al.* [94] investigated the recyclability of thermally treated PEEK powder, noting slight increases in crystallinity and significant changes in melt viscosity and flowability after treatment.

### 5.6. Economics and Scalability

SLS printing is expensive due to high printer costs, the need for skilled operators, and regular maintenance, making operational expenses significant. Scalability is a challenge, especially for large-scale production, and design constraints like minimum thickness and geometric complexity require advanced expertise. Hettesheimer *et al.* [95] analyzed the economic and energy impact of SLS in the automotive and aerospace industries. Despite high upfront costs, their study found that SLS offers substantial energy savings over its lifecycle, even for small components, highlighting its potential for long-term cost efficiency. Liu *et al.* [96] demonstrated a scalable method for producing flexible electronics using liquid metal and laser sintering. This technique, compatible with various substrates and automated processes, enables precise fabrication of multilayer and intricate circuits, proving the feasibility of scaling SLS technology for commercial applications.

### 5.7. Mitigation Strategies and Future Directions

Addressing these challenges requires a multifaceted approach that includes:

- Process Optimization: Refining laser power, scan speed, and layer thickness to enhance part quality and consistency.

- **Advanced Monitoring:** Employing real-time monitoring systems to detect and address defects during production.
- **Post-Processing Techniques:** Utilizing heat treatment, mechanical finishing, or surface coatings to improve part performance and aesthetics.
- **Material Innovations:** Developing new polymer materials with improved properties tailored for SLS applications.
- **Sustainability Practices:** Implementing powder regeneration techniques to reduce waste while ensuring material quality.

Despite its limitations, SLS remains a cornerstone of additive manufacturing due to its ability to produce complex geometries, functional prototypes, and customized components. Continued advancements in material science, process control, and post-processing are critical to expanding its industrial applicability and overcoming existing challenges.

In summary, SLS faces several challenges affecting its accuracy, surface quality, mechanical properties, material compatibility, and scalability. Dimensional inaccuracies arise from thermal shrinkage and residual stress, leading to warping and deviations, particularly along the Z-axis. Surface roughness is common due to the powder-based process, requiring post-processing like sanding or chemical treatments. Microstructural inconsistencies, such as porosity and anisotropy, weaken mechanical strength and require precise parameter control. Rapid thermal cycling induces residual stresses that can compromise mechanical properties, though heat treatments can improve strength and durability. Material limitations include sintering behavior, contamination risks, and degradation from excessive powder recycling. High costs, maintenance requirements, and scalability issues further hinder widespread adoption. To mitigate these challenges, strategies include optimizing process parameters, real-time defect monitoring, advanced post-processing, material innovations, and sustainable powder reuse. Despite these limitations, SLS remains a vital additive manufacturing technology, with ongoing advancements needed to enhance its efficiency and industrial viability.

## 6. Applications

SLS has become widely adopted across numerous industries due to its capability to fabricate intricate geometries and customized parts with high precision. Its adaptability makes it a preferred choice for applications requiring lightweight, durable, and highly tailored solutions. Table 1 lists key industries, their required properties, and the commonly used SLS materials.

In summary, SLS is widely used across various industries due to its ability to create complex, customized parts with high precision. Its versatility makes it ideal for lightweight, durable, and specialized applications. The growing range of SLS materials further enhances its adaptability and drives innovation.

## 7. Emerging Trends

SLS is evolving rapidly due to advancements other cutting-edge technologies. These developments are enhancing SLS's efficiency, broadening its applications, and enabling new capabilities. Fig. (21) highlights key emerging trends in SLS, including hybrid manufacturing, AI-driven processes, material innovations, automated post-processing, microstructure and property control, as well as process simulation and digital twin technologies.

### 7.1. Artificial Intelligence (AI) in SLS

AI is revolutionizing SLS through optimizing processes, improving part quality, and advancing design innovation.

#### 7.1.1. Process Optimization

AI algorithms enhance precision and efficiency in SLS by analyzing extensive data to optimize settings like laser power, scanning speed, and layer thickness. For example, Kim and Zohdi [108] demonstrated that deep learning

can predict optimal laser paths using minimal training data, with convolutional neural networks (CNNs) delivering faster simulations than traditional methods. Verma [109] used genetic algorithms to optimize part orientation, laser path planning, and layer thickness, reducing build time and volumetric error in direct metal laser sintering.

**Table 1: SLS applications and materials.**

Application	Required Properties	SLS Materials
Aerospace [97, 98]	High specific strength and stiffness, high-temperature resistance, toughness, corrosion resistance, vacuum compatibility	Polymers: PEEK, DuraForm PA, DuraForm EX. Metals: EOS Titanium Ti64, EOS Maraging Steel MS1, EOS Nickel Alloy IN718.
Automotive [98]	Weight reduction, safety, noise reduction, temperature tolerance, recyclability, mechanical properties	Polymers: ABS, PC, PEEK, Alumide, Nylon 11, 12, PA 640-GSL, PA6, PMMA, DuraForm PA, DuraForm GF, DuraForm EX, DuraForm HST, PA 850 Black. Metals and Composites: Al-SiC composites, EOS. Titanium Ti64, EOS Aluminum.
Biomedical implants [99-101]	Interconnected porosity, high density, strength, stiffness, bifunctionality, fatigue resistance, toughness, elasticity, corrosion resistance, biocompatibility	Metals: 316L Stainless Steel, CP-Titanium, Ti-6Al-4V, Ti-6Al-7Nb, CoCr alloys, EOS Titanium Ti64, EOS Cobalt Chrome MP1. Polymers: EOS PEEK HP3, UHMWPE, nylons, polycarbonate, polysulfone.
Prostheses [102]	Lightweight, durable, mimic natural functionality	Polymers: Prime Part, PA 1220/2201, PP, PMMA.
Dental [99]	High rigidity, strength, wear resistance, corrosion resistance, high-temperature resistance, biocompatibility	Metals: EOS Cobalt Chrome SP2, SP1, MP1, dental amalgams. Ceramics: Alumina, Zirconia, hydroxyapatite, tricalcium phosphate, pyrolytic carbon, bioglass. Others: Projet 6000, Projet MP 3000.
Hearing Aids [104, 106]	Rigid, durable, biocompatible, fine feature detailing	Polymers: Nylon polyamide, iPro 800 MP.
Tissue Engineering [99]	Biocompatibility	Polymers: PLA, PGA, PLGA.
Eyeglass Frames and Lenses [99, 103]	Lightweight, strong, flexible, optically clear	Frames: Nylon 11, Nylon 12. Lenses: PMMA.
Medical Devices [104, 105]	Biocompatibility, durability, weathering resistance, mechanical, thermal, and chemical properties	Polymers: PC, polyesters, ABS, PMMA, PP, HDPE, PVC.
Kitchenware, Housings, Covers, Containers [103]	Lightweight, tough, flexible, chemical resistance	LDPE, HDPE, PC, ABS, DuraForm GF, PA 640-GSL, PA 3200 GF, PP, PVC.
Art, Architectural Models, GIS, Hobby [106, 107]	Good surface finish, detailed features, chemical resistance, impact resistance, lightweight, excellent stiffness	Wax, plastics, DuraForm series, PA 650, PA 850 Black, PA 640-GSL, WindForm series powders, PA 250, PA-250 ACF

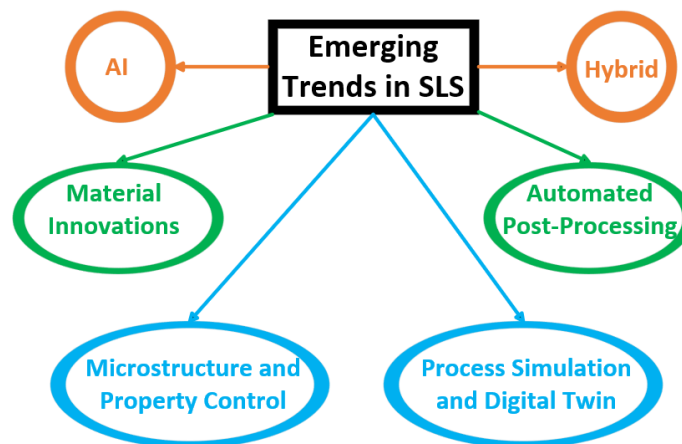


**Figure 21:** Emerging Trends in SLS.



AI-driven monitoring improves part quality by allowing for real-time adjustments to thermal conditions and material behavior. Abdalla *et al.* [110] employed machine learning (ML) to predict the printability of SLS formulations, using data from 170 formulations and inputs like material composition, FT-IR, XRPD, and DSC. Combining predictions from all data types into a consensus model achieved an F1 score of 88.9%, proving the benefits of multi-modal data integration. Similarly, Shen *et al.* [111] developed an artificial neural network (ANN) to predict the density of SLS parts based on process parameters. The ANN's predictions closely matched experimental results, confirming its accuracy.

By analyzing historical data, AI can predict potential issues and fine-tune processes, helping to prevent defects and minimize downtime. Tang *et al.* [112] introduced RCWGAN-GP, a machine learning algorithm capable of predicting microstructures without requiring governing laws. Trained on SEM micrographs of laser-sintered alumina, it accurately regenerated and predicted microstructure features like particle morphology and pore structure under various conditions. Tested with simulated data governed by the JMA equation, the algorithm reliably reproduced grain shapes, sizes, spatial distributions, and phase fractions, demonstrating its versatility.

### **7.1.2. Quality Control and Inspection**

AI-powered systems enhance quality control in additive manufacturing by detecting defects, optimizing processes, and ensuring consistency. Westphal and Seitz [113] developed transfer learning (TL) methods using pretrained convolutional neural networks (CNNs), VGG16 and Xception, to classify powder bed defects in the SLS process with small datasets. VGG16 achieved the best performance, with 95.8% accuracy and an AUC of 0.982, demonstrating the effectiveness of CNN-based TL for non-destructive defect detection and quality assurance.

Klamert *et al.* [114] applied deep learning (DL) for real-time quality control in SLS manufacturing, using the VGG16 CNN model to analyze infrared thermography data and detect induced defects. This approach achieved 98.54% accuracy in identifying curling failures, showcasing the potential of DL for in-situ defect detection.

AI is also used to evaluate surface roughness and mechanical properties in SLS. La Fé-Perdomo *et al.* [115] used machine learning (ML) models, including Multi-layer Perceptron, Support Vector Regression, and Random Forests, to analyze 316L metal parts. They examined how process parameters like laser power, scanning speed, hatch spacing, and layer thickness influence surface quality. While no single model excelled in predicting all properties, ensemble methods combining the best-performing models significantly improved accuracy.

### **7.1.3. Design Optimization**

AI enhances designs by reducing weight and material use while maintaining structural integrity. Guo *et al.* [116] introduced a semi-supervised deep learning framework (SSDLMA) to evaluate the manufacturability of metal cellular structures using direct metal laser sintering (DMLS). The method represents complex structures as 3D binary arrays through efficient voxelization and trains a deep learning classifier with minimal experimental data by leveraging semi-supervised learning. Comparisons with existing DFAM methods and machine learning models showed that SSDLMA offers superior accuracy and reliability. Notably, this framework can be adapted to assess the manufacturability of various complex geometries, even with limited training data.

## **7.2. Hybrid SLS Methods**

Hybrid approaches combine SLS with complementary technologies to address limitations, expand material capabilities, and broaden application potential.

### **7.2.1. SLS-Bio Fabrication**

Integrating SLS with bioprinting enables the production of complex biomedical implants and scaffolds, advancing tissue engineering and regenerative medicine. Tan *et al.* [117] studied biocompatible polymers, including PEEK, PVA, PCL, and PLLA, as well as the bio ceramic Hydroxyapatite (HA), optimizing SLS process parameters for these materials. Scaffold specimens created via SLS were analyzed using SEM. The micrographs confirmed the potential of these materials for constructing tissue engineering (TE) scaffolds, demonstrating the SLS process's ability to produce highly porous structures suitable for TE applications.

### 7.2.2. Hybrid Material Deposition

Combining SLS with Directed Energy Deposition (DED) or similar techniques enables localized reinforcement, material repair, and modification, enhancing component durability and adaptability. Tapoglou and Clulow [118] explored the production of complex geometries using a hybrid approach that combines additive and subtractive manufacturing techniques. They initially investigated the parameters for depositing stainless steel 316L, followed by an assessment of the machinability of the additively manufactured material. Finally, they conducted a thorough examination of the deposited and machined material's quality using a series of destructive and non-destructive methods.

### 7.2.3. In Situ Coating

Integrating techniques like chemical vapor deposition (CVD) or thermal spraying can apply functional coatings—such as thermal insulation, conductivity, or corrosion resistance—during or after printing, streamlining production and enhancing part performance. Zhang *et al.* [119] demonstrated this by preparing a SiO<sub>2</sub>@Si<sub>3</sub>N<sub>4</sub>ws-GPTMS core-shell filler. They grew silicon dioxide (SiO<sub>2</sub>) nanospheres on silicon nitride whiskers (Si<sub>3</sub>N<sub>4</sub>ws) *in situ* using a sol-gel method and modified the structure with the silane coupling agent GPTMS. The filler was then applied to the inner and outer surfaces of TPU skeletonized structural parts through vacuum dip coating with a water-based polyurethane (PU) coating, as shown in Fig. (22). Surface coating was finalized through warming and curing, enhancing the TPU parts via post-treatment.

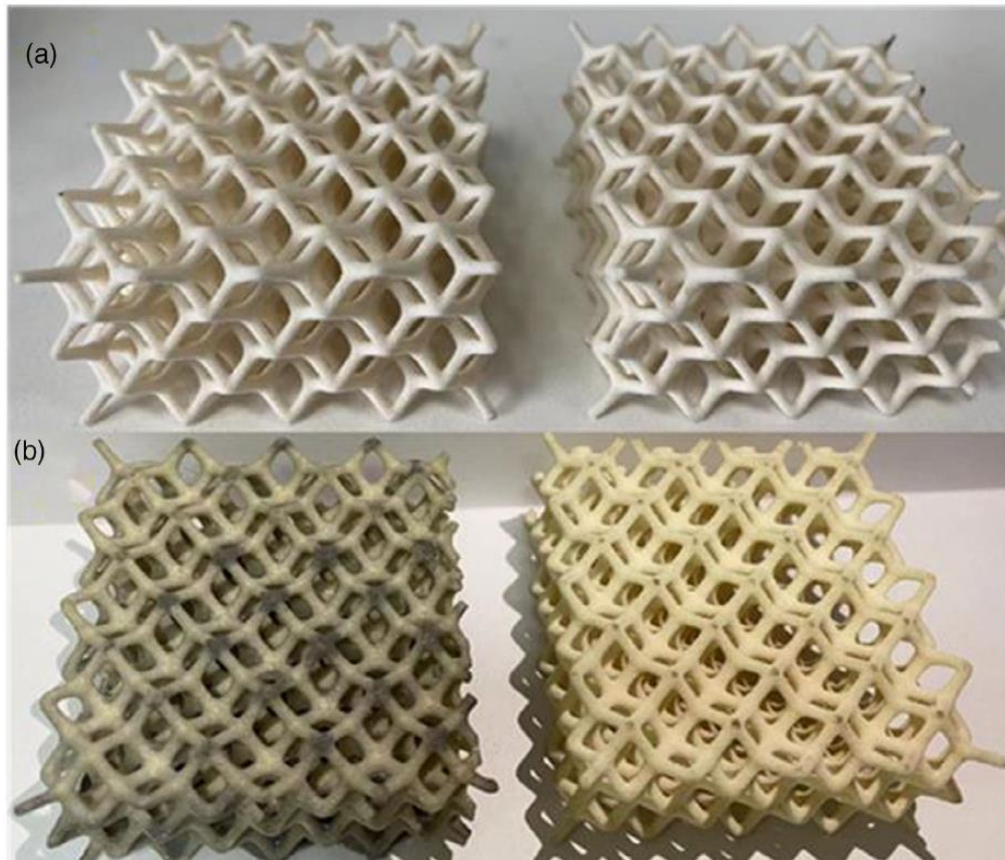


**Figure 22:** (a) Picture of pure TPU composite hollow structure printed parts; (b) Picture of TPU composite hollow structure filler coating [133].

### 7.3. Material Innovations in SLS

Advances in material science have broadened the capabilities of SLS, enabling the creation of durable, lightweight, and functional components for industries like aerospace, healthcare, and automotive. For example, Lexow and Drummer [120] explored modifying fine powders with flow agents to make powders with poor

flowability suitable for SLS. They also examined how antistatic agents influence powder flow and processing behavior. Even small amounts of additives significantly improved flow properties, allowing composite materials to be processed. This work provides valuable insights into dry particle coating mechanisms and their application in the expanding field of material development.

### 7.3.1. Advanced Polymers

New polymers with advanced properties like high-temperature resistance, biodegradability, and improved electrical or thermal conductivity are being developed for SLS. Yuan *et al.* [121] used experimental and theoretical methods to optimize processing for CNT-coated polyamide 12 (CNT/PA12) powders. These powders showed better heat conduction and absorption than pure polymer powders, extending the stable sintering range and enhancing the SLS process. Microstructural analysis revealed CNTs formed networks at powder boundaries, significantly boosting tensile strength, toughness, and elongation without reducing tensile modulus.

Aldahsh [122] introduced a composite of Polyamide 12 and cement to improve mechanical properties and lower costs. Thermal and mechanical tests (e.g., Young's modulus, tensile, flexural, compression, and impact strengths) were conducted with varying cement proportions to optimize SLS parameters. A casting method was also developed to quickly and cheaply produce test specimens with properties like SLS-made specimens. This research demonstrated that adding cement to Polyamide 12 produces stronger, more affordable sintered components than using pure Polyamide 12.

### 7.3.2. Multi-material Printing

Developing SLS systems capable of processing multiple materials simultaneously allow for the creation of composite parts with improved strength, stiffness, and durability. Mohan Krishna Sai *et al.* [123] demonstrated the fabrication of a multi-material laminate structure consisting of SS316, SS316 with 15% SiC by weight, and TiN using laser powder-bed fusion, highlighting significant property enhancements. FESEM analysis revealed key structural features, including the agglomeration of sintered powder particles, effective layer deposition, and columnar dendritic microstructures formed by directional solidification influenced by SiC and TiN particles.

The microhardness of the SS316 layer increased along the build direction, reflecting improved mechanical strength, while the SiC and TiN layers maintained consistent microhardness despite temperature differences. The coefficient of friction (COF) ranged from 0.137 to 0.128, indicating enhanced wear resistance. X-ray diffraction (XRD) analysis confirmed the formation of  $\alpha$ -iron (pearlite),  $\gamma$ -iron (austenite), Fe<sub>1.76</sub>Ni<sub>0.16</sub>, C<sub>1</sub>Cr<sub>2</sub>Fe<sub>14</sub>, and C<sub>0.8</sub>Cr<sub>0.579</sub>Mo<sub>0.42</sub> phases, which contributed to the improved mechanical and microstructural properties through chemical reactions between the materials in an argon atmosphere.

### 7.3.3. Functional Materials

SLS enables the fabrication of parts with specific functional properties, including biocompatibility. Kanczler *et al.* [124] investigated the biocompatibility of computationally designed surface selective laser sintering (SSLS) scaffolds as templates for promoting cell viability, growth, and osteogenesis. Using human fetal femur-derived cells, the study demonstrated successful cell culture on SSLS-poly(D,L)-lactic acid (SSLS-PLA) scaffolds, with alkaline phosphatase activity observed after seven days, indicating early osteogenic differentiation.

In both *in vitro* and *in vivo* models, the scaffolds supported cell proliferation, ingrowth, and matrix deposition, as evidenced by Alcian blue/Sirius red staining and type I collagen expression. When implanted into a murine critical-sized femur defect model, SSLS-PLA scaffolds, both alone and seeded with fetal femur-derived cells, facilitated bone regeneration. These findings highlight the potential of SSLS to create biocompatible and biodegradable scaffolds, precisely tailored to fit defects and provide a supportive template for osteogenesis in clinical applications.

### 7.3.4. Recycled and Sustainable Materials

With growing demand for sustainability, efforts are focused on recycling used powders and developing eco-friendly materials compatible with SLS to minimize waste. Wang *et al.* [125] investigated a sustainable composite

made from milled carbon fiber (mCF) and recycled polyamide 12 (rPA12) for extrusion additive manufacturing. The study found that mCF, composed of short, smooth fibers, did not significantly impact rPA12's thermal properties but moderately bonded with the polymer. Adding 30 wt.% mCF greatly improved the mechanical properties of rPA12, enhancing tensile, flexural, and impact strengths by up to 163%. These findings suggest that mCF/rPA12 composites offer a sustainable, high-performance material option for advanced manufacturing applications.

As material science continues to advance, we can expect to see even more innovative materials for SLS, further expanding the capabilities of this transformative technology.

#### 7.4. Automated Post-Processing

SLS scalability is improving with automation, making it more suitable for large-scale industrial use. Automated processes in heat treatment, polishing, and inspection are streamlining workflows and reducing manual labor. Lim and Pham [126] developed a fully automated vision system to classify and locate parts made with powder-based methods like SLS, binder jetting, and HP Multi Jet Fusion (MJF). The study introduced a method to simulate powder distribution on 3D-printed parts and use these simulated models in a deep learning system. The network trained on simulated powder models gave results similar to those trained on real images and performed better than networks using unpowdered CAD models. This method was especially effective for parts that differed from their CAD models due to powder buildup, demonstrating how simulated data can improve automated inspection.

With this automation, SLS and other powder-based manufacturing processes are becoming more efficient and reliable for industrial applications.

#### 7.5. Microstructure and Property Control

##### 7.5.1. Advanced Laser Systems

New laser configurations, such as multi-beam systems, offer better control over microstructure, leading to denser, more uniform parts with less thermal distortion. Zhang *et al.* [127] studied AlSi10Mg samples produced with a multi-laser selective laser melting (SLM) system, focusing on relative density, defects, microstructure, and mechanical properties in isolated and overlapping areas.

The study found that melt pools in the overlapping areas were wider and deeper than in isolated areas, creating clear boundaries at the overlaps. Small pores were seen along these boundaries but had little impact on material properties. Both isolated and overlapping regions had similar microstructures, microhardness, and tensile strength. After annealing, the silicon changed from dendrites to particles without causing grain growth, so there were minimal differences in strength due to consistent grain size. This shows that multi-laser setups can improve production efficiency without sacrificing quality, which is important for high-throughput manufacturing.

Heeling and Wegener [128] found that using a second laser beam to heat the area around the melt pool helped to evenly distribute temperature, slow cooling, and improve wetting behavior. Their study shows that this approach can lead to better surface quality and denser microstructures with less remelting.

##### 7.5.2. Rapid Cooling Techniques

Non-equilibrium solidification methods, like martensitic transformations, enhance microstructures for better mechanical performance. Chen *et al.* [129] realized a direct preparation of complete lath martensite microstructure (transformation rate  $\delta > 99\%$ ) in tool steel using selective laser melting (SLM) in conjunction with laser remelting (LR) technique. Ultrafine lath martensite with a high percentage of low-angle grain boundaries (LAGBs) (46.12%) was formed. This unique microstructure contributed to the prominent effect of dislocation rearrangement and entanglement within the substructure of martensite, leading to a significant improvement of mechanical properties. An ultrahigh microhardness of  $\sim 765.1 \text{ HV}_{0.3}$  was obtained, which is much higher than the previously reported values of as-built SLM hardened steel such as H13 steel and maraging steel.

## 7.6. Process Simulation and Digital Twin

Advanced digital tools are transforming SLS process simulation and monitoring.

### 7.6.1. Simulation Models

Sophisticated computational models help predict and optimize process outcomes, reducing the need for trial-and-error experiments. Yang *et al.* [130] developed a numerical model that incorporates entropy levels, non-isothermal kinetics, and heat transfer equations coupled with microstructure evolution. The model also accounts for partial melting and laser-powder interactions. They performed 3D finite element simulations of a single SLS scan, using a new algorithm to manage the high computational cost and simulate 200 grains with just 8 non-conserved order parameters. Applying this model to SLS of stainless steel 316L powder, they identified how laser power and scan speed affect microstructural features like porosity, surface morphology, temperature, grain geometry, and densification. The model also validated the kinetics of transient porosity during densification and showed its ability to predict the relationship between densification and specific energy input during SLS.

### 7.6.2. Digital Twin Technology

Real-time virtual replicas of SLS systems improve predictive analytics, allowing for smarter production control. Hermann *et al.* [131] introduced a new concept using a digital twin to move towards a fully software-defined and predictable laser metal deposition process. This concept integrates machine data with data-driven machine learning models and physics-based simulations, enabling more accurate predictions of single track geometries. The approach was validated on a laser metal deposition machine.

These emerging trends are transforming SLS into a cutting-edge technology capable of addressing complex manufacturing challenges. Through the integration of AI, hybrid methods, material innovations, scalability improvements, microstructure control, and digital tools, SLS is poised for broader adoption and impactful contributions across various industries.

In summary, SLS is rapidly advancing due to developments in artificial intelligence (AI), hybrid manufacturing, material innovations, and automated post-processing. AI enhances SLS processes by improving precision, predicting defects, and ensuring better part quality through deep learning and machine learning algorithms. It aids in process optimization, real-time monitoring, quality control, and design innovation, ensuring efficient and reliable production. Hybrid SLS methods combine complementary technologies like bioprinting, directed energy deposition (DED), and *in situ* coating, expanding material capabilities and applications, especially in biomedical and structural engineering. Material innovations, including advanced polymers, multi-material printing, functional materials, and sustainable options, are broadening SLS's potential in aerospace, healthcare, and automotive industries. Researchers are working on high-temperature-resistant polymers, composites, and biocompatible scaffolds, while sustainability efforts emphasize recycling and eco-friendly materials. Additionally, automated post-processing techniques, such as heat treatment, polishing, and AI-driven inspection, are streamlining workflows and reducing labor. Together, these advancements improve SLS efficiency, scalability, and range of applications, reinforcing its role as a transformative manufacturing technology.

## 8. Conclusion

In conclusion, SLS has significantly advanced the production of complex, high-performance components across various industries. However, several challenges remain, including dimensional accuracy, surface roughness, residual stress, limited material options, and high post-processing requirements. Future research should focus on improving material properties, refining process parameters, and integrating advanced monitoring technologies, such as AI, to enhance real-time control and defect prediction. Additionally, exploring hybrid manufacturing approaches and developing new high-performance materials will further expand SLS capabilities, enabling broader adoption in aerospace, automotive, and medical applications.

## Conflict of Interest

The authors declare that they have no conflicts of interest related to the present study.

## Funding

The authors received no specific funding for this study.

## Acknowledgments

The authors would like to express their sincere gratitude to Dr. Peiqin Zhang at Texas State University for her support in this study.

## References

- [1] Deckard C. Method and apparatus for producing parts by selective sintering. U.S. Patent No. 4,863,538. 1989.
- [2] Das S. Physical aspects of process control in selective laser sintering of metals. *Adv Eng Mater.* 2003; 5(10): 701-11. <https://doi.org/10.1002/adem.200310099>
- [3] Zhang S, Tang H, Tang D, Liu T, Liao W. Effect of fabrication process on the microstructure and mechanical performance of carbon fiber reinforced PEEK composites via selective laser sintering. *Compos Sci Technol.* 2024; 246: 110396. <https://doi.org/10.1016/j.compscitech.2023.110396>
- [4] Wu Z, Shi C, Chen A, Li Y, Chen S, Sun D, *et al.* Large-scale, abrasion-resistant, and solvent-free superhydrophobic objects fabricated by a selective laser sintering 3D printing strategy. *Adv Sci.* 2023; 10(9): 2207183. <https://doi.org/10.1002/advs.202207183>
- [5] Zhang Y, Thakkar R, Zhang J, Lu A, Duggal I, Pillai A, *et al.* Investigating the use of magnetic nanoparticles as alternative sintering agents in selective laser sintering (SLS) 3D printing of oral tablets. *ACS Biomater Sci Eng.* 2023; 9(6): 2924-36. <https://doi.org/10.1021/acsbomaterials.2c00299>
- [6] Deng K, Wu H, Li Y, Jiang J, Wang M, Yang Z, Zhang R. The resin-ceramic-based Fe<sub>3</sub>O<sub>4</sub>/graphite composites rapidly fabricated by selective laser sintering for integration of structural-bearing and broadband electromagnetic wave absorption. *J Alloys Compd.* 2023; 943: 169120. <https://doi.org/10.1016/j.jallcom.2023.169120>
- [7] Wu Z, Sun D, Shi C, Chen S, Tang S, Li Y, *et al.* Moisture-thermal stable, superhydrophilic alumina-based ceramics fabricated by a selective laser sintering 3D printing strategy for solar steam generation. *Adv Funct Mater.* 2023; 33: 2304897. <https://doi.org/10.1002/adfm.202304897>
- [8] Xue C, Li N, Chen S, Liang J, Aiyiti W. The laser selective sintering controlled forming of flexible TPMS structures. *Materials.* 2023; 16(24): 7565. <https://doi.org/10.3390/ma16247565>
- [9] Choudhury D, Ponneganti S, Radhakrishnanand P, Murty US, Banerjee S. Selective laser sintering additive manufacturing of solid oral dosage form: Effect of laser power and hatch spacing on the physico-technical behaviour of sintered printlets. *Appl Mater Today.* 2023; 35: 101943. <https://doi.org/10.1016/j.apmt.2023.101943>
- [10] Ghaltaghchyan T, Khachatryan H, Asatryan K, Rstakyan V, Aghayan M. Effect of additives on selective laser sintering of silicon carbide. *Bol Soc Esp Ceram Vidr.* 2023; 62(6): 504-14. <https://doi.org/10.1016/j.bsecv.2023.01.001>
- [11] Han W, Kong L, Xu M. Advances in selective laser sintering of polymers. *Int J Extrem Manuf.* 2022; 4: 042002. <https://doi.org/10.1088/2631-7990/ac9096>
- [12] Hassan MS, Billah KMM, Hall SE, Sepulveda S, Regis JE, Marquez C, *et al.* Selective laser sintering of high-temperature thermoset polymer. *J Compos Sci.* 2022; 6(2): 41. <https://doi.org/10.3390/jcs6020041>
- [13] Shi Y, Li Z, Huang S, Zeng F. Effect of the properties of the polymer materials on the quality of selective laser sintering parts. *Proc Inst Mech Eng L J Mater Des Appl.* 2014; 218(3): 247-52. <https://doi.org/10.1243/1464420041579454>
- [14] Gibson I, Shi D. Material properties and fabrication parameters in selective laser sintering process. *Rapid Prototyp J.* 1997; 3(4): 129-36. <https://doi.org/10.1108/13552549710191836>
- [15] Tiwari SK, Pande S, Agrawal S, Bobade SM. Selection of selective laser sintering materials for different applications. *Rapid Prototyp J.* 2015; 21(6): 630-48. <https://doi.org/10.1108/RPJ-03-2013-0027>
- [16] Storch S, Nellessen D, Schaefer G, Reiter R. Selective laser sintering: qualifying analysis of metal-based powder systems for automotive applications. *Rapid Prototyp J.* 2003; 9(4): 240-51. <https://doi.org/10.1108/13552540310489622>
- [17] Elbadawi M, Li H, Ghosh P, Alkahtani ME, Lu B, Basit AW, *et al.* Cold laser sintering of medicines: toward carbon-neutral pharmaceutical printing. *ACS Sustain Chem Eng.* 2024; 12: 11155-66. <https://doi.org/10.1021/acssuschemeng.4c01439>
- [18] Williams JV, Revington PJ. Novel use of an aerospace selective laser sintering machine for rapid prototyping of an orbital blowout fracture. *Int J Oral Maxillofac Surg.* 2010; 39(2): 182-4. <https://doi.org/10.1016/j.ijom.2009.12.002>

- [19] Lv Y, Thomas W, Chalk R, Hewitt A, Singamneni S. Polyetherimide powders as material alternatives for selective laser-sintering components for aerospace applications. *J Mater Res.* 2020; 35(23-24): 3222-34. <https://doi.org/10.1557/jmr.2020.317>
- [20] Quincieu J, Robinson C, Stucker B, Mosher T. Case study: selective laser sintering of the USUSat II small satellite structure. *Assem Autom.* 2005; 25(4): 267-72. <https://doi.org/10.1108/01445150510626389>
- [21] Goulas A, Friel RJ. Laser sintering of ceramic materials for aeronautical and astronautical applications. In: Brandt M, editor. *Laser additive manufacturing.* Woodhead Publishing; 2017. pp. 373-98. <https://doi.org/10.1016/B978-0-08-100433-3.00014-2>
- [22] Agarwala S, Goh GL, Truong-Son DL, An J, Peh ZK, Yeong WY, *et al.* Wearable bandage-based strain sensor for home healthcare: combining 3D aerosol jet printing and laser sintering. *ACS Sens.* 2019; 4(1): 218-26. <https://doi.org/10.1021/acssensors.8b01293>
- [23] Awad A, Fina F, Goyanes A, Gaisford S, Basit AW. 3D printing: principles and pharmaceutical applications of selective laser sintering. *Int J Pharm.* 2020; 586: 119594. <https://doi.org/10.1016/j.ijpharm.2020.119594>
- [24] Fina F, Goyanes A, Gaisford S, Basit AW. Selective laser sintering (SLS) 3D printing of medicines. *Int J Pharm.* 2017; 529(1-2): 285-93. <https://doi.org/10.1016/j.ijpharm.2017.06.082>
- [25] Tel A, Kornfellner E, Molnár E, Johannes S, Moscato F, Robiony M. Selective laser sintering at the point-of-care 3D printing laboratory in hospitals for cranio-maxillo-facial surgery: a further step into industrial additive manufacturing made available to clinicians. *Ann 3D Print Med.* 2024; 16: 100175. <https://doi.org/10.1016/j.stlm.2024.100175>
- [26] Yan CZ, Shi YS, Yang JS, Xu L. Preparation and selective laser sintering of nylon-12-coated aluminum powders. *Journal of composite materials.* 2009;43(17):1835-51
- [27] Subramanian K, Vail N, Barlow J, Marcus H. Selective laser sintering of alumina with polymer binders. *Rapid Prototyp J.* 1995; 1(2): 24-35. <https://doi.org/10.1108/13552549510086844>
- [28] Harada Y, Ishida Y, Miura D, Watanabe S, Aoki H, Miyasaka T, *et al.* Mechanical properties of selective laser sintering pure titanium and Ti-6Al-4V, and its anisotropy. *Materials.* 2020; 13(22): 5081. <https://doi.org/10.3390/ma13225081>
- [29] Yan M, Tian X, Peng G, Li D, Yao R, Zhang W, *et al.* Performance study of lightweight composites equipment section support fabricated by selective laser sintering. *J Mech Eng.* 2019; 55(13): 144-50. <https://doi.org/10.3901/JME.2019.13.144>
- [30] Özbay Kısasöz B, Serhatlı IE, Bulduk ME. Selective laser sintering manufacturing and characterization of lightweight PA 12 polymer composites with different hollow microsphere additives. *J Mater Eng Perform.* 2022; 31(5): 4049-59. <https://doi.org/10.1007/s11665-021-06481-x>
- [31] Chen X, Yin J, Liu X, Pei B, Huang J, Peng X, *et al.* Effect of laser power on mechanical properties of SiC composites rapidly fabricated by selective laser sintering and direct liquid silicon infiltration. *Ceram Int.* 2022; 48(13): 19123-31. <https://doi.org/10.1016/j.ceramint.2022.03.203>
- [32] Zhu W, Yan C, Shi Y, Wen S, Liu J, Wei Q, *et al.* A novel method based on selective laser sintering for preparing high-performance carbon fibers/polyamide12/epoxy ternary composites. *Sci Rep.* 2016; 6: 33780. <https://doi.org/10.1038/srep33780>
- [33] Azam MU, Belyamani I, Schiffer A, Kumar S, Askar K. Progress in selective laser sintering of multifunctional polymer composites for strain- and self-sensing applications. *J Mater Res Technol.* 2024; 30: 9625-46. <https://doi.org/10.1016/j.jmrt.2024.06.024>
- [34] Yuan Y, Wu W, Hu H, Liu D, Shen H, Wang Z. The combination of Al<sub>2</sub>O<sub>3</sub> and BN for enhancing the thermal conductivity of PA12 composites prepared by selective laser sintering. *RSC Adv.* 2021; 11: 1984-91. <https://doi.org/10.1039/D0RA09775F>
- [35] Singh S, Kaur D, Singh M, Balu R, Mehta A, Vasudev H. Challenges and issues in manufacturing of components using polymer-based selective laser sintering (SLS): a review. *Int J Interact Des Manuf.* 2024; 1-24. <https://doi.org/10.1007/s12008-024-02049-w>
- [36] Han W, Kong L, Xu M. Advances in selective laser sintering of polymers. *Int J Extrem Manuf.* 2022; 4: 042002. <https://doi.org/10.1088/2631-7990/ac9096>
- [37] Petzold S, Klett J, Schauer A, Osswald TA. Surface roughness of polyamide 12 parts manufactured using selective laser sintering. *Polym Test.* 2019; 80: 106094. <https://doi.org/10.1016/j.polymertesting.2019.106094>
- [38] Tonello R, Conradsen K, Pedersen DB, Frisvad JR. Surface roughness and grain size variation when 3D printing polyamide 11 parts using selective laser sintering. *Polymers.* 2023; 15(13): 2967. <https://doi.org/10.3390/polym15132967>
- [39] Sachdeva A, Singh S, Sharma VS. Investigating surface roughness of parts produced by SLS process. *Int J Adv Manuf Technol.* 2013; 64: 1505-16. <https://doi.org/10.1007/s00170-012-4118-z>
- [40] Impey S, Saxena P, Salonitis K. Selective laser sintering induced residual stresses: precision measurement and prediction. *J Manuf Mater Process.* 2021; 5(3): 101. <https://doi.org/10.3390/jmmp5030101>
- [41] Van Zyl I, Yadroitsava I, Yadroitsev I. Residual stress in Ti6Al4V objects produced by direct metal laser sintering. *S Afr J Ind Eng.* 2016; 27(4): 134-41. <https://doi.org/10.7166/27-4-1468>
- [42] Lamikiz A, Sánchez JA, López de Lacalle LN, Arana JL. Laser polishing of parts built up by selective laser sintering. *Int J Mach Tools Manuf.* 2007; 47(12): 2040-50. <https://doi.org/10.1016/j.ijmachtools.2007.01.013>
- [43] Sanz C, García Navas V. Structural integrity of direct metal laser sintered parts subjected to thermal and finishing treatments. *J Mater Process Technol.* 2007; 213(12): 2126-36. <https://doi.org/10.1016/j.jmatprotec.2013.06.013>
- [44] Chivel Y, Smurov I. On-line temperature monitoring in selective laser sintering/melting. *Phys Procedia.* 2010; 5: 515-21. <https://doi.org/10.1016/j.phpro.2010.08.079>

- [45] Gardner MR, Lewis A, Jongwan P, McElroy AB, Estrada AD, Fish S, *et al.* *In situ* process monitoring in selective laser sintering using optical coherence tomography. *Opt Eng.* 2018; 57(4): 1-5. <https://doi.org/10.1117/1.OE.57.4.041407>
- [46] Zhang L, Phillips T, Mok A, Moser D, Beaman J. Automatic laser control system for selective laser sintering. *IEEE Trans Ind Inform.* 2019; 15(4): 2177-85. <https://doi.org/10.1109/TII.2018.2867007>
- [47] Abdalla Y, Ferienc M, Awad A, Kim J, Elbadawi M, Basit AW, *et al.* Smart laser sintering: deep learning-powered powder bed fusion 3D printing in precision medicine. *Int J Pharm.* 2024; 661(15): 124440. <https://doi.org/10.1016/j.ijpharm.2024.124440>
- [48] Yehia HM, Hamada A, Sebaey TA, Abd-Elaziem W. Selective laser sintering of polymers: process parameters, machine learning approaches, and future directions. *J Manuf Mater Process.* 2024; 8: 19. <https://doi.org/10.3390/jmmp8050197>
- [49] Lupone F, Padovano E, Ostrovskaya O, Russo A, Badini C. Innovative approach to the development of conductive hybrid composites for selective laser sintering. *Compos Part A Appl Sci Manuf.* 2021; 147: 106429. <https://doi.org/10.1016/j.compositesa.2021.106429>
- [50] Ferreira JAM, Santos LMS, da Silva J, Costa JM, Capela C. Assessment of the fatigue life on functional hybrid laser sintering steel components. *Procedia Struct Integr.* 2016; 1: 126-33. <https://doi.org/10.1016/j.prostr.2016.02.018>
- [51] Leu MC, Pattnaik S, Hilmas GE. Investigation of laser sintering for freeform fabrication of zirconium diboride parts. *Virtual Phys Prototyp.* 2012; 7(1): 25-36. <https://doi.org/10.1080/17452759.2012.666119>
- [52] Goodridge RD, Tuck CJ, Hague RJ. Laser sintering of polyamides and other polymers. *Prog Mater Sci.* 2012; 57(2): 229-67. <https://doi.org/10.1016/j.pmatsci.2011.04.001>
- [53] Lupone F, Padovano E, Casamento F, Badini C. Process phenomena and material properties in selective laser sintering of polymers: a review. *Materials.* 2022; 15: 183. <https://doi.org/10.3390/ma15010183>
- [54] Miao G, Du W, Pei Z, Ma C. A literature review on powder spreading in additive manufacturing. *Addit Manuf.* 2022; 58: 103029. <https://doi.org/10.1016/j.addma.2022.103029>
- [55] Yang Y, Ragnvaldsen O, Bai Y, Yi M, Xu BX. Three-dimensional non-isothermal phase-field modeling of microstructure evolution during selective laser sintering. *Comput Mater.* 2019; 5: 8. <https://doi.org/10.1038/s41524-019-0219-7>
- [56] Polivnikova T. Study and modelling of the melt pool dynamics during selective laser sintering and melting [doctoral dissertation]. Lausanne: EPFL; 2015.
- [57] Benedetti L, Brulé B, Decraemer N, Evans KE, Ghita O. Evaluation of particle coalescence and its implications in laser sintering. *Powder technology.* 2019;342:917-28
- [58] Soldner D, Steinmann P, Mergheim J. Modeling crystallization kinetics for selective laser sintering of polyamide 12. *GAMM-Mitt.* 2021; 44(3): e202100011. <https://doi.org/10.1002/gamm.202100011>
- [59] Agarwala M, Bourell D, Beaman J, Marcus H, Barlow J. Post-processing of selective laser sintered metal parts. *Rapid Prototyp J.* 1995; 1(2): 36-44. <https://doi.org/10.1108/13552549510086853>
- [60] Zarringhalam H, Hopkinson N, Kamperman N, De Vlieger J. Effects of processing on microstructure and properties of SLS Nylon 12. *Mater Sci Eng A.* 2006; 435: 172-80. <https://doi.org/10.1016/j.msea.2006.07.084>
- [61] Chung H, Das S. Functionally graded Nylon-11/silica nanocomposites produced by selective laser sintering. *Mater Sci Eng A.* 2008; 487: 251-7. <https://doi.org/10.1016/j.msea.2007.10.082>
- [62] Zhu W, Yan C, Shi Y, Wen S, Han C, Cai C, *et al.* Study on the selective laser sintering of a low-isotacticity polypropylene powder. *Rapid Prototyp J.* 2016; 22(4): 621-9. <https://doi.org/10.1108/RPJ-02-2015-0014>
- [63] Guo Y, Chen H, Tian S, Xu Y, Ma K, Ma S, *et al.* Investigation of the ageing conditions of PEEK powder for the selective laser sintering process. *Virtual Phys Prototyp.* 2023; 18(1): e2273298. <https://doi.org/10.1080/17452759.2023.2273298>
- [64] Zhang C, Wu W, Hu H, Rui Z, Ye J, Shen H. Effect of multidimensional filler hybridization on the mechanical properties of thermoplastic polyurethane composites prepared by selective laser sintering. *J Appl Polym Sci.* 2023; 140(28): 1-14. <https://doi.org/10.1002/app.54041>
- [65] Xie F, He X, Cao S, Qu X. Structural and mechanical characteristics of porous 316L stainless steel fabricated by indirect selective laser sintering. *J Mater Process Technol.* 2013; 213: 838-43. <https://doi.org/10.1016/j.jmatprotec.2012.12.014>
- [66] Olakanmi EO, Cochrane RF, Dalgarno KW. Densification mechanism and microstructural evolution in selective laser sintering of Al-12Si powders. *J Mater Process Technol.* 2011; 211: 113-21. <https://doi.org/10.1016/j.jmatprotec.2010.09.003>
- [67] Fischer P, Locher M, Romano V, Weber HP, Kolossov S, Glardon R. Temperature measurements during selective laser sintering of titanium powder. *Int J Mach Tools Manuf.* 2004; 12: 1293-6. <https://doi.org/10.1016/j.ijmactools.2004.04.019>
- [68] Dejan S, Kosovka O, Rebeka R, Rajko B, Dragoslav S. Selective laser melting and sintering technique of the cobalt-chromium dental alloy. *Srp Arh Celok Lek.* 2023; 147(11-12): 664-9. <https://doi.org/10.2298/SARH190706112S>
- [69] Akhtar S, Wright CS, Youseffi M, Hauser C, Childs THC, Taylor CM, *et al.* Direct selective laser sintering of tool steel powders to high density: part B - the effect on microstructural evolution. *Int Solid Freeform Fabr Symp.* 2003; 656-67.
- [70] Shahzad K, Deckers J, Kruth JP, Vleugels J. Additive manufacturing of alumina parts by indirect selective laser sintering and post processing. *J Mater Process Technol.* 2013; 213: 1484-94. <https://doi.org/10.1016/j.jmatprotec.2013.03.014>
- [71] Abdelmoula M, Küçüktürk G, Grossin D, Zarazaga AM, Maury F, Ferrato M. Direct selective laser sintering of silicon carbide: realizing the full potential through process parameter optimization. *Ceram Int.* 2023; 49(20): 32426-39. <https://doi.org/10.1016/j.ceramint.2023.07.189>



- [72] Shahzad K, Deckers J, Zhang Z, Kruth JP, Vleugels J. Additive manufacturing of zirconia parts by indirect selective laser sintering. *J Eur Ceram Soc.* 2014; 34(1): 81-9. <https://doi.org/10.1016/j.jeurceramsoc.2013.07.023>
- [73] Shuai C, Feng P, Cao C, Peng S. Processing and characterization of laser sintered hydroxyapatite scaffold for tissue engineering. *Biotechnol Bioprocess Eng.* 2013; 18: 520-7. <https://doi.org/10.1007/s12257-012-0508-1>
- [74] Olakanmi EO, Cochrane RF, Dalgarno KW. A review on selective laser sintering/melting (SLS/SLM) of aluminum alloy powders: processing, microstructure, and properties. *Prog Mater Sci.* 2015; 74: 401-77. <https://doi.org/10.1016/j.pmatsci.2015.03.002>
- [75] Gharate T, Karanwad T, Lekurwale S, Banerjee S. Effect of laser power ratios on sinterability and physical properties of 3D prototypes sintered using selective laser sintering. *J 3D Print Med.* 2023; 7(3): 3DP011. <https://doi.org/10.2217/3dp-2023-0007>
- [76] Vande Ryse R, Edeleva M, Van Stichel O, D'hooge DR, Pille F, Fiorio R, *et al.* Setting the optimal laser power for sustainable powder bed fusion processing of elastomeric polyesters: a combined experimental and theoretical study. *Materials.* 2022; 15: 385. <https://doi.org/10.3390/ma15010385>
- [77] Kozak J, Zakrzewski T. Accuracy problems of additive manufacturing using SLS/SLM processes. *AIP Conf Proc.* 2018; 2017(1): 1-12. <https://doi.org/10.1063/1.5056273>
- [78] Bian P, Shi J, Liu Y, Xie Y. Influence of laser power and scanning strategy on residual stress distribution in additively manufactured 316L steel. *Opt Laser Technol.* 2021; 132: 106477. <https://doi.org/10.1016/j.optlastec.2020.106477>
- [79] Hou G, Yu Z, Ye D. The influence of laser power and scanning speed on the dimensional accuracy of SLS formed parts. *IOP Conf Ser Earth Environ Sci.* 2021; 791: 1-9. <https://doi.org/10.1088/1755-1315/791/1/012154>
- [80] Jain PK, Pandey PM, Rao PVM. Experimental investigations for improving part strength in selective laser sintering. *Virtual Phys Prototyp.* 2008; 3(3): 177-88. <https://doi.org/10.1080/17452750802065893>
- [81] Chatterjee AN, Kumar S, Saha P, Mishra PK, Choudhury AR. An experimental design approach to selective laser sintering of low carbon steel. *J Mater Process Technol.* 2003; 136(1-3): 151-7. [https://doi.org/10.1016/S0924-0136\(03\)00132-8](https://doi.org/10.1016/S0924-0136(03)00132-8)
- [82] Danezan A, Delaizir G, Tessier-Doyen N, Gasgnier G, Gaillard JM, Duport P, *et al.* Selective laser sintering of porcelain. *J Eur Ceram Soc.* 2018; 38(2): 769-75. <https://doi.org/10.1016/j.jeurceramsoc.2017.09.034>
- [83] Li XF, Dong JH. Study on curve of pre-heating temperature control in selective laser sintering. *Proc Int Symp Web Inf Syst Appl. (WISA'09)* 2009; 156-8.
- [84] Sachdeva A, Singh S, Sharma VS. Investigating surface roughness of parts produced by SLS process. *Int J Adv Manuf Technol.* 2013; 64: 1505-16. <https://doi.org/10.1007/s00170-012-4118-z>
- [85] Low KH, Leong KF, Chua CK, Du ZH, Cheah CM. Characterization of SLS parts for drug delivery devices. *Rapid Prototyp J.* 2001; 7(5): 262-8. <https://doi.org/10.1108/13552540110410468>
- [86] Sofia D, Chirona R, Lettieri P, Barletta D, Poletto M. Selective laser sintering of ceramic powders with bimodal particle size distribution. *Chem Eng Res Des.* 2018; 136: 536-47. <https://doi.org/10.1016/j.cherd.2018.06.008>
- [87] Czelusniak T, Amorim FL. Selective laser sintering of carbon fiber-reinforced PA12: Gaussian process modeling and stochastic optimization of process variables. *Int J Adv Manuf Technol.* 2020; 110: 2049-66. <https://doi.org/10.1007/s00170-020-05993-5>
- [88] Abdelmoula M, Küçüktürk G, Grossin D, Zarazaga AM, Maury F, Ferrato M. Direct selective laser sintering of silicon carbide: realizing the full potential through process parameter optimization. *Ceram Int.* 2023; 49: 32426-39. <https://doi.org/10.1016/j.ceramint.2023.07.189>
- [89] Singh S, Sachdeva A, Sharma VS. Investigation of dimensional accuracy/mechanical properties of part produced by selective laser sintering. *Int J Appl Sci Eng.* 2012; 10(1): 59-68.
- [90] Beard MA, Ghita OR, Evans KE. Using Raman spectroscopy to monitor surface finish and roughness of components manufactured by selective laser sintering. *J Raman Spectrosc.* 2011; 42: 744-8. <https://doi.org/10.1002/jrs.2771>
- [91] Salmoria GV, Leite JL, Paggi RA. The microstructural characterization of PA6/PA12 blend specimens fabricated by selective laser sintering. *Polym Test.* 2009; 28: 746-51. <https://doi.org/10.1016/j.polymertesting.2009.06.010>
- [92] Balan GS, Raj SA, Adithya R. Effect of post-heat treatment on the mechanical and surface properties of nylon 12 produced via material extrusion and selective laser sintering processes. *Polym Bull.* 2024; 2: 1-26. <https://doi.org/10.1007/s00289-024-05197-x>
- [93] Toncheva A, Brison L, Dubois P, Laoutid F. Recycled tire rubber in additive manufacturing: selective laser sintering for polymer-ground rubber composites. *Appl Sci.* 2021; 11: 8778. <https://doi.org/10.3390/app11188778>
- [94] Patel A, Venoor V, Yang F, Chen X, Sobkowicz MJ. Evaluating poly (ether ether ketone) powder recyclability for selective laser sintering applications. *Polym Degrad Stab.* 2021; 185: 109502. <https://doi.org/10.1016/j.polymdegradstab.2021.109502>
- [95] Hetteshheimer T, Hirzel S, Roß HB. Energy savings through additive manufacturing: an analysis of selective laser sintering for automotive and aircraft components. *Energy Effic.* 2018; 11: 1227-45. <https://doi.org/10.1007/s12053-018-9620-1>
- [96] Liu S, Yuen MC, White EL, Boley JW, Deng B, Cheng GJ, Kramer-Bottiglio R. Laser sintering of liquid metal nanoparticles for scalable manufacturing of soft and flexible electronics. *ACS Appl Mater Interfaces.* 2018; 10(33): 28232-41. <https://doi.org/10.1021/acsami.8b08722>
- [97] Kobryn PA, Ontko NR, Perkins LP, Tiley JS. Additive manufacturing of aerospace alloys for aircraft structures. *Cost Effective Manuf Net-Shape Process, Meet Proc (RTO-MP-AVT-139)* 2006; 3.
- [98] Rao PR. *Advances in materials and their applications.* New Delhi: New Age International Publishers; 2009.
- [99] Wong JY, Bronzino JD. *Biomaterials.* Boca Raton: CRC Press; 2007. <https://doi.org/10.1201/9780849378898>

- [100] Xiang L, Chengtao W, Wenguang Z, Yuanchao L. Fabrication and compressive properties of Ti6Al4V implant with honeycomb-like structure for biomedical applications. *Rapid Prototyp J.* 2010; 16(1): 44-9. <https://doi.org/10.1108/13552541011011703>
- [101] Williams DF. On the mechanisms of biocompatibility. *Biomaterials* 2008; 29(20): 2941-53. <https://doi.org/10.1016/j.biomaterials.2008.04.023>
- [102] Wu G, Zhou B, Bi Y, Zhao Y. Selective laser sintering technology for customized fabrication of facial prostheses. *J Prosthet Dent.* 2008; 100: 56-60. [https://doi.org/10.1016/S0022-3913\(08\)60138-9](https://doi.org/10.1016/S0022-3913(08)60138-9)
- [103] Kalpakjian S, Schmid SR. *Manufacturing engineering and technology.* 8<sup>th</sup> ed. Upper Saddle River: Pearson Publishing Company; 2020.
- [104] Tiwari SK, Pande S. Material properties and selection for selective laser sintering process. *Int J Manuf Technol Manag.* 2013; 27(4-6): 198-217. <https://doi.org/10.1504/IJMTM.2013.058904>
- [105] Ouellette J. Biomaterials facilitate medical breakthroughs. *Ind Phys.* 2001; 7(5): 18-21.
- [106] Wong KV, Hernandez A. A review of additive manufacturing. *ISRN Mech Eng.* 2012; 2012: 208760. <https://doi.org/10.5402/2012/208760>
- [107] Gibson I, Rosen WD, Stucker B. *Additive manufacturing technologies: 3D printing, rapid prototyping and direct digital manufacturing.* 2<sup>nd</sup> ed. UK: Springer Publishers; 2014. <https://doi.org/10.1007/978-1-4939-2113-3>
- [108] Kim DH, Zohdi T. Tool path optimization of selective laser sintering processes using deep learning. *Comput Mech.* 2022; 69(1): 383-401. <https://doi.org/10.1007/s00466-021-02079-1>
- [109] Verma AP. Minimizing build time and surface inaccuracy of direct metal laser sintered parts: an artificial intelligence-based optimization approach [master's thesis]. Cincinnati: University of Cincinnati; 2009. Available from: [http://rave.ohiolink.edu/etdc/view?acc\\_num=ucin1249840383](http://rave.ohiolink.edu/etdc/view?acc_num=ucin1249840383)
- [110] Abdalla Y, Elbadawi M, Ji M, Alkahtani M, Awad A, Orlu M, *et al.* Machine learning using multi-modal data predicts the production of selective laser sintered 3D printed drug products. *Int J Pharm.* 2023; 633: 122628. <https://doi.org/10.1016/j.ijpharm.2023.122628>
- [111] Shen X, Yao J, Wang Y, Yang J. Density prediction of selective laser sintering parts based on artificial neural network. In: *Advances in neural networks-ISNN 2004: International Symposium on Neural Networks*, Dalian, China, August 19-21, 2004, Proceedings, Part II. Berlin Heidelberg: Springer; 2004. p. 832-40. [https://doi.org/10.1007/978-3-540-28648-6\\_133](https://doi.org/10.1007/978-3-540-28648-6_133)
- [112] Tang J, Geng X, Li D, Shi Y, Tong J, Xiao H, *et al.* Machine learning-based microstructure prediction during laser sintering of alumina. *Sci Rep.* 2021; 11(1): 1-10. <https://doi.org/10.1038/s41598-021-89816-x>
- [113] Westphal E, Seitz H. A machine learning method for defect detection and visualization in selective laser sintering based on convolutional neural networks. *Addit Manuf.* 2021; 41: 101965. <https://doi.org/10.1016/j.addma.2021.101965>
- [114] Klamert V, Schmid-Kietreiber M, Bublin M. A deep learning approach for real-time process monitoring and curling defect detection in selective laser sintering by infrared thermography and convolutional neural networks. *Procedia CIRP.* 2022; 111: 317-20. <https://doi.org/10.1016/j.procir.2022.08.030>
- [115] La Fé-Perdomo I, Ramos-Grez JA, Jeria I, Guerra C, Barrionuevo GO. Comparative analysis and experimental validation of statistical and machine learning-based regressors for modeling the surface roughness and mechanical properties of 316L stainless steel specimens produced by selective laser melting. *J Manuf Process.* 2022; 80: 666-82. <https://doi.org/10.1016/j.jmapro.2022.06.021>
- [116] Guo Y, Lu WF, Fuh JYH. Semi-supervised deep learning-based framework for assessing manufacturability of cellular structures in direct metal laser sintering process. *J Intell Manuf.* 2021; 32(2): 347-59. <https://doi.org/10.1007/s10845-020-01575-0>
- [117] Tan KH, Chua CK, Leong KF, Cheah CM, Gui WS, Tan WS, *et al.* Selective laser sintering of biocompatible polymers for applications in tissue engineering. *Biomed Mater Eng.* 2005; 15(1-2): 113-24.
- [118] Tapoglou N, Clulow J. Investigation of hybrid manufacturing of stainless steel 316L components using direct energy deposition. *Proc Inst Mech Eng B J Eng Manuf.* 2020; 235(10): 1633-43. <https://doi.org/10.1177/0954405420949360>
- [119] Zhang C, Wu W, Hu H, Rui Z, Ye J, Wang Z, *et al.* Preparation of SiO<sub>2</sub>/Si<sub>3</sub>N<sub>4</sub>/PU reinforced coating and its reinforcement mechanism for SLS-molded TPU materials. *J Appl Polym Sci.* 2023; 140(35): e54355. <https://doi.org/10.1002/app.54355>
- [120] Lexow MM, Drummer D. New materials for SLS: the use of antistatic and flow agents. *J Powder Technol.* 2016; 2016: 4101089. <https://doi.org/10.1155/2016/4101089>
- [121] Yuan S, Chua CK, Zhou K, Bai J, Wei J. Material evaluation and process optimization of CNT-coated polymer powders for selective laser sintering. *Polymers.* 2018; 8: 370. <https://doi.org/10.3390/polym8100370>
- [122] Aldahsh S. Development of a new composite powder material of cement additive with polyamide 12 for selective laser sintering [doctoral dissertation]. Cardiff: Cardiff University; 2016. Available from: <https://orca.cardiff.ac.uk/id/eprint/10948>
- [123] Mohan Krishna Sai M, Kumar S, Mandal A, Anand M. Sinterability of SS316, SiC, and TiN multi-material additive manufacturing via selective laser sintering. *Opt Laser Technol.* 2023; 167: 109686. <https://doi.org/10.1016/j.optlastec.2023.109686>
- [124] Kanczler JM, Mirmalek-Sani S, Hanley NA, Ivanov AL, Barry JJA, Upton C, *et al.* Biocompatibility and osteogenic potential of human fetal femur-derived cells on surface selective laser sintered scaffolds. *Acta Biomater.* 2017; 5(6): 2063-71. <https://doi.org/10.1016/j.actbio.2009.03.010>
- [125] Wang L, Kiziltas A, Mielewski DF, Lee EC, Gardner DJ. Closed-loop recycling of polyamide12 powder from selective laser sintering into sustainable composites. *J Clean Prod.* 2018; 195(10): 765-72. <https://doi.org/10.1016/j.jclepro.2018.05.235>
- [126] Lim JXY, Pham QC. Automated post-processing of 3D-printed parts: artificial powdering for deep classification and localization. *Virtual Phys Prototyp.* 2021; 2833(1): 30008-14.

- [127] Zhang C, Zhu H, Hu Z, Zhang L, Zeng X. A comparative study on single-laser and multi-laser selective laser melting AlSi10Mg: defects, microstructure and mechanical properties. *Mater Sci Eng A*. 2019; 746: 416-23. <https://doi.org/10.1016/j.msea.2019.01.024>
- [128] Heeling T, Wegener K. The effect of multi-beam strategies on selective laser melting of stainless steel 316L. *Addit Manuf*. 2018; 22: 334-42. <https://doi.org/10.1016/j.addma.2018.05.026>
- [129] Chen H, Gu D, Dai D, Xia M, Ma C. A novel approach to direct preparation of complete lath martensite microstructure in tool steel by selective laser melting. *Mater Lett*. 2018; 227(15): 128-31. <https://doi.org/10.1016/j.matlet.2018.05.042>
- [130] Yang Y, Ragnvaldsen O, Bai Y, Yi M, Xu BX. 3D non-isothermal phase-field simulation of microstructure evolution during selective laser sintering. *npj Comput Mater*. 2023; 5(1): 81. <https://doi.org/10.1038/s41524-019-0219-7>
- [131] Hermann F, Chen B, Ghasemi G, Stegmaier V, Ackermann T, Reimann P, *et al*. A digital twin approach for the prediction of the geometry of single tracks produced by laser metal deposition. *Procedia CIRP*. 2022; 107: 83-8. <https://doi.org/10.1016/j.procir.2022.04.014>